JOC Article

Synthesis and Properties of Oligo[*n*]cruciforms: Nanosized Sterically Encumbered Tetraethynylphenyl-Homologated Fluorophores

Abdelaziz Al Ouahabi,[†] Paul N. W. Baxter,*[,†] Jean-Paul Gisselbrecht,[‡] André De Cian,[§] Lydia Brelot,[§] and Nathalie Kyritsakas-Gruber[§,||]

Institut Charles Sadron, CNRS UPR 022, 6 rue du Loess, F-67083 Strasbourg, France, and Laboratoire d'Electrochimie et de Chimie Physique du Corps Solide, Service de Radiocrystallographie, CNRS UMR 7177, and Laboratoire de Chimie de Coordination Organique, CNRS UMR 7140, Institut Le Bel, Université Louis Pasteur, 4 rue Blaise Pascal, F-67070 Strasbourg, France

baxter@ics.u-strasbg.fr

Received December 23, 2008

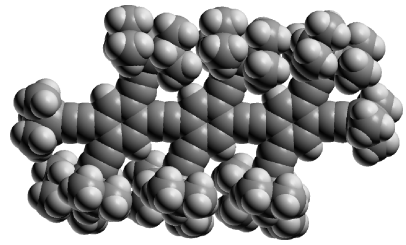

A series of nanosized phenyleneethynylenes have been prepared which are sterically insulated from the surrounding environment by multiple functionalization with triisopropylsilyl (TIPS) substituents. The phenyleneethynylenes comprise oligo[*n*]cruciforms **1**−**4** ($n = 3-5$) and a dehydrotribenzo[12]annulene **5**, the former of which possess *para*-acyclic and the latter *ortho*-cyclic electronic conjugation pathways. All compounds were characterized by ^{1}H and ^{13}C NMR, IR, and mass spectroscopic techniques. The X-ray crystal structure of **1** confirmed the sterically isolating properties of the TIPS substituents. A comparison of the physical properties of these electronically differing systems revealed that they were all luminescent upon UV irradiation displayed negligible aggregation in dilute solution and that particular members of the series studied were electrochemically active, undergoing facile reversible reductions. The phenyleneethynylenes also exhibited significantly enhanced thermal stability by virtue of the presence of the TIPS substituents. The properties of **1**−**5** suggest that they are promising building blocks for the construction of materials for novel molecular electronics applications.

Introduction

Since the first report of doping-induced electrical conductivity in polyacetylene in the 1970s,[1a,b] the synthesis and study of conjugated organic polymers has rapidly developed into a field of major technological and economic importance.[2a−d] Electronic components and devices incorporating organic polymers offer many advantages over those fabricated from traditional inorganic and metallic materials in that the former are lightweight, resistant to corrosion, and mechanically robust. Organic polymers can also be easily processed into thin films of varying thickness and topology via solvent evaporation, spin coating, etc. and may be directly functionalized with, e.g., biomaterials or quantum dots, and used in sensing applications.[3a−j] In particular, conjugated organic polymers are now of significant commercial importance for the construction of organic light emitting diodes (OLEDs), thin film transistors (TFTs), and field effect transistors (FETs), which are finding applications in computing hardware and electronic appliances.[4a−f]

[†] Institut Charles Sadron.

[‡] Laboratoire d'Electrochimie et de Chimie Physique du Corps Solide, Université Louis Pasteur.

[§] Service de Radiocrystallographie, Université Louis Pasteur.

[||] Current address: Laboratoire de Chimie de Coordination Organique, Université Louis Pasteur.

(1) (a) Etemad, S.; Heeger, A. J.; MacDiarmid, A. G. *Annu. Rev. Phys. Chem.* **1982**, *33*, 443–469. (b) MacDiarmid, A. G.; Heeger, A. J. *Synth. Met.* **1980**, *1*, 101–118.

(2) (a) Kiebooms, R.; Menon, R.; Lee, K. In *Handbook of Advanced Electronic and Photonic Materials and Devices: Vol. 8 Conducting Polymers*; Nalwa, H. S., Ed.; Academic Press: New York, 2001. (b) Skotheim, T. A., Elsenbaumer, R. L., Reynolds, J. R., Ed. *Handbook of Conducting Polymers*, 2nd ed.; Dekker: New York, 1998. (c) Nalwa, H. S., Ed. *Handbook of Organic Conductive Molecules and Polymers*; Wiley: New York, 1997; Vols. *1*−*4*. (d) Skotheim, T. A., Ed. *Handbook of Conducting Polymers*; Dekker: New York, 1986; Vols. 1 and 2.

10.1021/jo802797e CCC: $40.75 © 2009 American Chemical Society
Published on Web 06/12/2009

An important physicochemical property displayed by the majority of conjugated organic oligomers and polymers is that of luminescence both in solution and the solid state when irradiated with light of particular wavelengths. For OLEDs, the luminescence is generated electrically, and it is of special importance to tune the conjugation of the oligomer/polymer in a controllable way in order to obtain electroluminescence of a desired color.

For both electrically and light-stimulated emission, surprisingly little is currently understood about how the relative alignments between the oligomer/polymer chains and the detailed nature of their interchain contacts affect their physical properties such as luminescence color, quantum yield, and electrochemical behavior.[5a−e] The overall efficiency of OLEDs is determined by both the charge transport and emissive properties of the materials used, however it is clear that short interchain contacts such as aromatic stacking will favor charge transport but may significantly decrease the overall luminescence quantum yield.

In general, short interchain contacts would thus facilitate luminescence energy transfer between oligomer/polymer chains and maximize the chance of loss in energy as heat. The excitons would also be able to hop between polymer chains enabling the preferred light re-emission from the chromophores of lowest energy. This effect is observed with blended mixtures of different chromophores which emit light only from the chromophore of lowest energy, thereby preventing the possibility of luminescence color tuning by mixing chromophores of differing emission energies.[6]

One way of increasing the luminescence emission efficiency of conjugated organic polymers and oligomers would be to increase the interchain distances by encapsulation in media transparent to light,[7a−c] or alternatively to protect the chains as rotaxanes or wrapped inside helical polysaccharides.[8a−c] Both approaches have had some success, although the former avenue provides little control of interchain contacts at a molecular level while the latter may be synthetically demanding. A third approach is to synthesize conjugated polymers and oligomers with sterically bulky substituents covalently attached either to the main backbone or capping the chain ends. Such substituents are often branched or dendritic and serve to both increase solubility and minimize interchain contacts.[8b,9a,b]

In the case of OLEDs, however, if conjugated systems are too isolated, then the efficiency of interchain charge transport would be reduced. With long polymers, significant charge transport would be possible along the polymer chains, and the negative effects of isolation upon the charge transport would be less severe. An alternative approach would also be to construct block copolymers comprising segments which may engage in aromatic stacking interactions to aid interchain charge transport and sterically isolated segments to enhance emission efficiency.

One of the most highly studied and synthetically accessible classes of conjugated organic polymers is that of the polyphenylethynylenes.[10] They have been prepared with a diverse range of different substituents for the purpose of developing new types of OLEDs, sensors, redox, antenna, and photoconducting and photorefractive materials. Recently, a class of molecular phenyleneethynylenes comprising 1,2,4,5-tetraarylethynylbenzenes and 1,2-diarylethynyl-4,5-diarylethenylbenzenes, known as cruciforms, have been the focus of a surge in interest due to their

(3) For reviews on the sensing applications of conjugated polymers, see for example: (a) Thomas, S. W., III; Joly, G. D.; Swager, T. M. *Chem. Rev.* **2007**, *107*, 1339–1386. (b) Achyuthan, K. E.; Bergstedt, T. S.; Chen, L.; Jones, R. M.; Kumaraswamy, S.; Kushon, S. A.; Ley, K. D.; Lu, L.; McBranch, D.; Mukundan, H.; Rininsland, F.; Shi, X.; Xia, W.; Whitten, D. G. *J. Mater. Chem.* **2005**, *15*, 2648–2656. (c) Leclerc, M.; Ho, H.-A. *Synlett* **2004**, 380–387. (d) Liu, B.; Bazan, G. C. *Chem. Mater.* **2004**, *16*, 4467–4476. (e) Pinto, M. R.; Schanze, K. S. *Synthesis* **2002**, 1293–1309. (f) Leclerc, M. *Adv. Mater.* **1999**, *11*, 1491–1498. (g) Okada, S.; Peng, S.; Spevak, W.; Charych, D. *Acc. Chem. Res.* **1998**, *31*, 229–239. For metal/inorganic nanoparticle-conjugated oligomer/polymer assemblies, see: (h) Zotti, G.; Vercelli, B.; Berlin, A. *Chem. Mater.* **2008**, *20*, 6509–6516. (i) Bensebaa, F.; Farah, A. A.; Wang, D.; Bock, C.; Du, X.; Kung, J.; Le Page, Y. *J. Phys. Chem. B* **2005**, *109*, 15339–15344. (j) Cassagneau, T.; Mallouk, T. E.; Fendler, J. H. *J. Am. Chem. Soc.* **1998**, *120*, 7848–7859.

(4) For reviews and reports on OLEDs, see: (a) Anderson, S. *Chem.—Eur. J.* **2001**, *7*, 4706–4714. (b) Mitschke, U.; Bäuerle, P. *J. Mater. Chem.* **2000**, *10*, 1471–1507. (c) Friend, R. H.; Gymer, R. W.; Holmes, A. B.; Burroughes, J. H.; Marks, R. N.; Taliani, C.; Bradley, D. D. C.; Dos Santos, D. A.; Brédas, J. L.; Lögdlund, M.; Salaneck, W. R. *Nature* **1999**, *397*, 121–128. (d) Kraft, A.; Grimsdale, A. C.; Holmes, A. B. *Angew. Chem., Int. Ed.* **1998**, *37*, 402–428. For a review on OTFTs, see: (e) Dimitrakopoulos, C. D.; Malenfant, P. R. L. *Adv. Mater.* **2002**, *14*, 99–117. For a review on OFETs, see: (f) Horowitz, G. *Adv. Mater.* **1998**, *10*, 365–377.

(5) (a) Lacroix, J. C.; Chane-Ching, K. I.; Maquère, F.; Maurel, F. *J. Am. Chem. Soc.* **2006**, *128*, 7264–7276. (b) Knoblock, K. M.; Silvestri, C. J.; Collard, D. M. *J. Am. Chem. Soc.* **2006**, *128*, 13680–13681. (c) Cornil, J.; Beljonne, D.; Calbert, J.-P.; Brédas, J.-L. *Adv. Mater.* **2001**, *13*, 1053–1067. (d) Cornil, J.; Calbert, J.-P.; Beljonne, D.; Silbey, R.; Brédas, J.-L. *Synth. Met.* **2001**, *119*, 1–6. (e) Schweikart, K.-H.; Hohloch, M.; Steinhuber, E.; Hanack, M.; Lüer, L.; Gierschner, J.; Egelhaaf, H.-J.; Oelkrug, D. *Synth. Met.* **2001**, *121*, 1641–1642.

(6) Adronov, A.; Fréchet, J. M. J. *Chem. Commun.* **2000**, 1701–1710.

(7) (a) Spange, S. *Angew. Chem., Int. Ed.* **2003**, *42*, 4430–4432. (b) Calzaferri, G.; Huber, S.; Maas, H.; Minkowski, C. *Angew. Chem., Int. Ed.* **2003**, *42*, 3732–3758. (c) Lin, V. S.-Y.; Radu, D. R.; Han, M.-K.; Deng, W.; Kuroki, S.; Shanks, B. H.; Pruski, M. *J. Am. Chem. Soc.* **2002**, *124*, 9040–9041.

(8) (a) Frampton, M. J.; Claridge, T. D. W.; Latini, G.; Brovelli, S.; Cacialli, F.; Anderson, H. L. *Chem. Commun.* **2008**, 2797–2799. (b) Frampton, M. J.; Anderson, H. L. *Angew. Chem. Int. Ed* **2007**, *46*, 1028–1064, and references cited therein. (c) Eelkema, R.; Maeda, K.; Odell, B.; Anderson, H. L. *J. Am. Chem. Soc.* **2007**, *129*, 12384–12385.

(9) (a) Englert, B. C.; Smith, M. D.; Hardcastle, K. I.; Bunz, U. H. F. *Macromolecules* **2004**, *37*, 8212–8221. (b) Gibtner, T.; Hampel, F.; Gisselbrecht, J.-P.; Hirsch, A. *Chem.—Eur. J.* **2002**, *8*, 408–432.

(10) Bunz, U. H. F. *Chem. Rev.* **2000**, *100*, 1605–1644.

(11) The majority of work reported to date concerns cruciforms constructed from single, non-oligomeric 1,2,4,5-tetrasubstituted benzene cores which we have called [1]cruciforms. For recent examples of the spectroscopic and electrochemical properties of [1]cruciforms, see: (a) Samori, S.; Tojo, S.; Fujitsuka, M.; Spitler, E. L.; Haley, M. M.; Majima, T. *J. Org. Chem.* **2008**, *73*, 3551–3558. (b) Wilson, J. N.; Hardcastle, K. I.; Josowicz, M.; Bunz, U. H. F. *Tetrahedron* **2004**, *60*, 7157–7167. (c) Wilson, J. N.; Smith, M. D.; Enkelmann, V.; Bunz, U. H. F. *Chem. Commun.* **2004**, 1700–1701. (d) Wilson, J. N.; Josowicz, M.; Wang, Y.; Bunz, U. H. F. *Chem. Commun.* **2003**, 2962–2963. (e) Klare, J. E.; Tulevski, G. S.; Sugo, K.; de Picciotto, A.; White, K. A.; Nuckolls, C. *J. Am. Chem. Soc.* **2003**, *125*, 6030–6031. (f) Diederich, F.; Philp, D.; Seiler, P. *J. Chem. Soc., Chem. Commun.* **1994**, 205–208. For sensory applications of [1]cruciform fluorophores, see: (g) McGrier, P. L.; Solntsev, K. M.; Miao, S.; Tolbert, L. M.; Miranda, O. R.; Rotello, V. M.; Bunz, U. H. F. *Chem.—Eur. J.* **2008**, *14*, 4503–4510. (h) McGrier, P. L.; Solntsev, K. M.; Schönhaber, J.; Brombosz, S. M.; Tolbert, L. M.; Bunz, U. H. F. *Chem. Commun.* **2007**, 2127–2129. (i) Spitler, E. L.; Shirtcliff, L. D.; Haley, M. M. *J. Org. Chem.* **2007**, *72*, 86–96. (j) Hauck, M.; Schönhaber, J.; Zucchero, A. J.; Hardcastle, K. I.; Müller, T. J. J.; Bunz, U. H. F. *J. Org. Chem.* **2007**, *72*, 6714–6725. (k) Brombosz, S. M.; Zucchero, A. J.; Phillips, R. L.; Vazquez, D.; Wilson, A.; Bunz, U. H. F. *Org. Lett.* **2007**, *9*, 4519–4522. (l) Zucchero, A. J.; Wilson, J. N.; Bunz, U. H. F. *J. Am. Chem. Soc.* **2006**, *128*, 11872–11881. (m) Wilson, J. N.; Bunz, U. H. F. *J. Am. Chem. Soc.* **2005**, *127*, 4124–4125. For the metallo-assembly of prisms and polymers incorporating [1]cruciforms, see: (n) Caskey, D. C.; Yamamoto, T.; Addicott, C.; Shoemaker, R. K.; Vacek, J.; Hawkridge, A. M.; Muddiman, D. C.; Kottas, G. S.; Michl, J.; Stang, P. J. *J. Am. Chem. Soc.* **2008**, *130*, 7620–7628. (o) Gerhardt, W. W.; Zucchero, A. J.; South, C. R.; Bunz, U. H. F.; Weck, M. *Chem.—Eur. J.* **2007**, *13*, 4467–4474. (p) Gerhardt, W. W.; Zucchero, A. J.; Wilson, J. N.; South, C. R.; Bunz, U. H. F.; Weck, M. *Chem. Commun.* **2006**, 2141–2143. (q) Manimaran, B.; Thanasekaran, P.; Rajendran, T.; Liao, R.-T.; Liu, Y.-H.; Lee, G.-H.; Peng, S.-M.; Rajagopal, S.; Lu, K.-L. *Inorg. Chem.* **2003**, *42*, 4795–4797. For the use of [1]cruciforms for the construction of switches, nanoparticle and multimagnetic assemblies, see: (r) Grunder, S.; Huber, R.; Horhoiu, V.; González, M. T.; Schönenberger, C.; Calame, M.; Mayor, M. *J. Org. Chem.* **2007**, *72*, 8337–8344. (s) Lim, I.-I. S.; Vaiana, C.; Zhang, Z.-Y.; Zhang, Y.-J.; An, D.-L.; Zhong, C.-J. *J. Am. Chem. Soc.* **2007**, *129*, 5368–5369. (t) Amoroso, A. J.; Cargill Thompson, A. M. W.; Maher, J. P.; McCleverty, J. A.; Ward, M. D. *Inorg. Chem.* **1995**, *34*, 4828–4835. For the construction of a [1]cruciform "carborane-wheeled nanocar" for the exploration of nanomechanical motions, see: (u) Morin, J.-F.; Sasaki, T.; Shirai, Y.; Guerrero, J. M.; Tour, J. M. *J. Org. Chem.* **2007**, *72*, 9481–9490.

SCHEME 1. Synthesis of Sterically Encumbered Oligocruciforms 1−4[a]

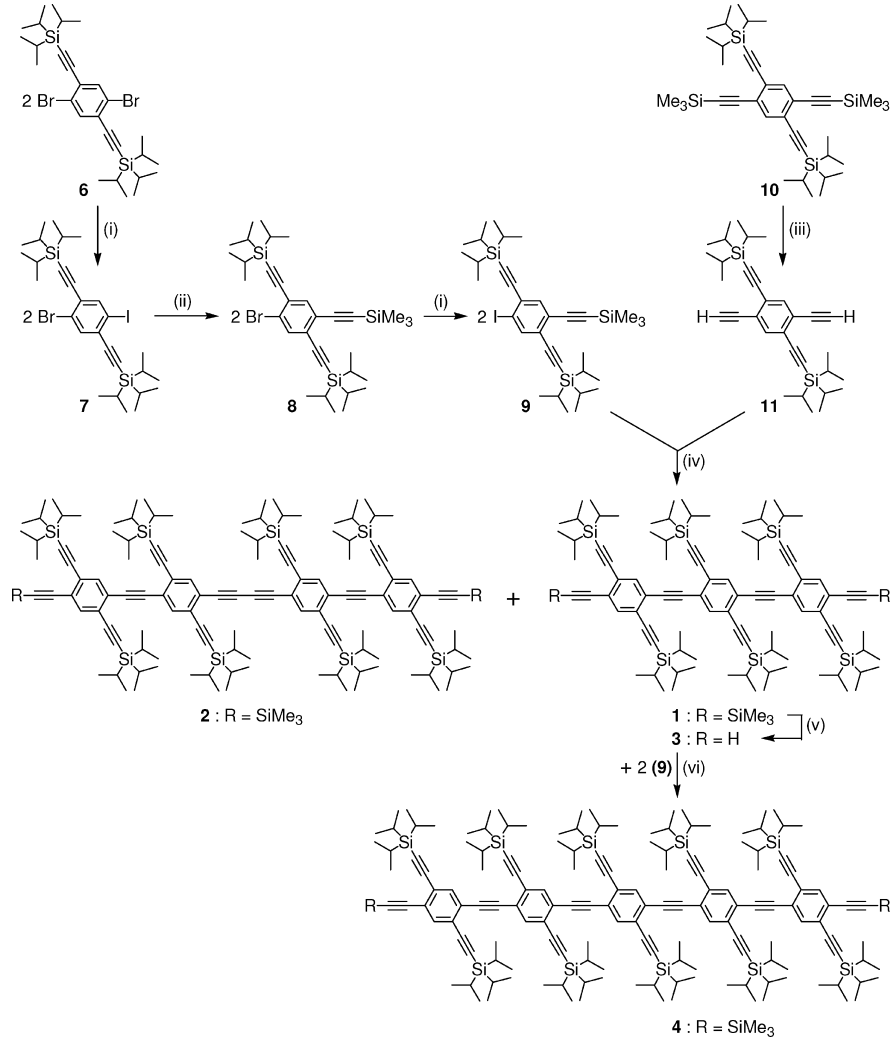

[a] Key: (i) *n*-BuLi, Et_2O, −78 °C, 1.5−2 h then ICH_2CH_2I/Et_2O, −78 °C, 4 h (76% **7**), (80% **9**); (ii) TMSA, $[PdCl_2(PPh_3)_2]$, CuI cat., toluene/Et_3N, 20 °C, 7 d (77% **8**); (iii) K_2CO_3, MeOH, 20 °C, 4 d, (77% **11**);[16] (iv) $[PdCl_2(dppf)]\cdot CH_2Cl_2$, CuI cat., toluene/$Et_3N$, 20 °C, 14−19 d (64% **1**, argon), (52% **1**, 10% **2**, argon/air 80: 20); (v) K_2CO_3, 4:1 THF/MeOH, 20 °C, 7 d (94% **3**); (vi) $[PdCl_2(dppf)]\cdot CH_2Cl_2$, CuI cat., toluene/$Et_3N$, 20 °C, 4 d then 60 °C, 5 d (17% **4**).

fascinating luminescent and sensory properties and potential use in nanomechanical machines.[11a−u]

With the aforementioned considerations in mind, we therefore reasoned that oligomeric strings of conjugated cruciforms comprising *para*-connected 1,2,4,5-tetraethynylbenzene units functionalized with sterically bulky substituents would exhibit physicochemical properties characteristic of single molecules, unperturbed by effects resulting from intermolecular aggregation and associations. They would therefore function as ideal models for studying the effect of steric isolation at a molecular level on their electronic and spectroscopic properties[12] and in particular serve as promising candidates for the creation of OLED polymers and block copolymers with enhanced emission characteristics.

We decided to prepare the sterically encumbered TIPS-substituted oligocruciforms **1**−**4** shown in Scheme 1, as molecular modeling showed that the TIPS groups would prevent intermolecular contacts between the alkynyl and benzenoid portions of each oligomer.

The fact that the TIPS substituents are lipophilic would also be expected to significantly assist the solubility of the larger oligomers and their lack of conjugation and saturation further reduce the ease of intermolecular exciton hopping in these systems. Furthermore, the use of 1,2,4,5-tetraethynylbenzene units extends the chromophoric surface area of the oligomers and increases the conjugation of the phenylethynylene backbone. Oligo[*n*]cruciforms of this type where $n \geq 1$ would therefore be expected to yield chromophores with superior luminescence emission properties. The TIPS substituents were also anticipated to increase the stability of the chromophores toward degradation by heat and light, an expectation that was born out upon subsequent exploration of their properties. The fulfillment of this latter requirement is important if real-life applications are to be found for such materials.[13a−e]

In order to expand our studies to include sterically encumbered phenyleneethynylenes with alternative conjugation pathways to that of the *para*-/cross-conjugation of **1**−**4**, we prepared the TIPS-functionalized dehydrotribenzo[12]annulene **5** (Scheme

(12) Reports of oligo[*n*]cruciforms are rare in the literature, see, for example: (a) An oligo[2]cruciform comprising two 1,2,4,5-tetraethynylbenzene subunits with a 1,4-butadiyne bridge, used as a precursor for the syntheses of acediynes: Gallagher, M. E.; Anthony, J. E. *Tetrahedron Lett.* **2001**, *42*, 7533–7536. For an oligo[2]cruciform incorporating extended TTF units with a 1,4-butadiyne bridge, see: (b) Vestergaard, M.; Jennum, K.; Sørensen, J. K.; Kilså, K.; Nielsen, M. B. *J. Org. Chem.* **2008**, *73*, 3175–3183.

SCHEME 2. Synthesis of Sterically Encumbered Dehydrotribenzo[12]annulene 5[a]

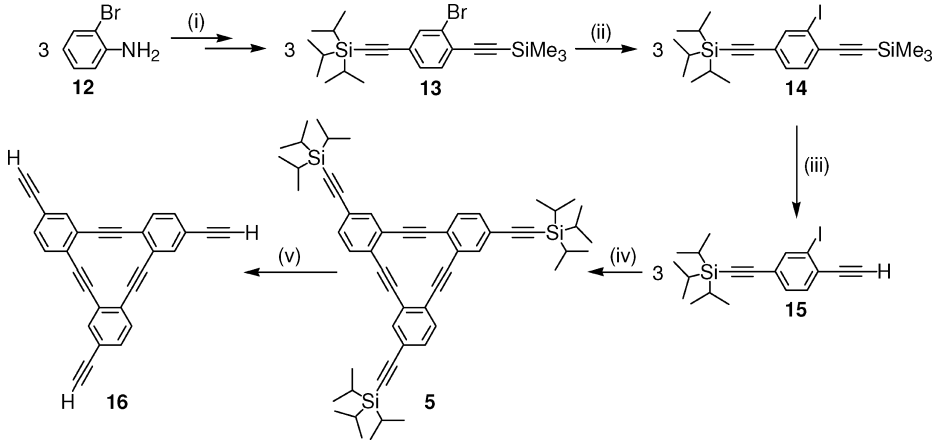

[a] Key: (i) five steps;[22] (ii) *n*-BuLi, Et_2O, −78 °C, 1.5 h then ICH_2CH_2I/Et_2O, −78 °C, 3 h (95% **14**); (iii) K_2CO_3, 0.6:1 THF/MeOH, 20 °C, 14 h (98% **15**); (iv) 1: 2 mol ratio of **15**: *t*-BuOCu, pyridine, 35−40 °C, 4 h, then 125 °C−140 °C, 10 h (20% **5**); (v) $[(n\text{-}Bu)_4N]F$/THF, 20 °C, 48 h (94% **16**).

2). Compound **5** offers the opportunity for investigating the electronic and spectroscopic effects of steric encumbrance on a cyclically *ortho*-conjugated analogue of **1** which possesses the same number of benzene rings.

Results and Discussion

Oligomer Synthesis and Characterization. The sterically isolated oligocruciforms **1**−**4** were synthesized according to the reaction sequence shown in Scheme 1. Thus, the halogen−lithium exchange reaction of **6**[14] in Et_2O solution at low temperature resulted in clean monolithiation when treated with 1 equiv of *n*-BuLi. Subsequent quenching of the monolithiophenyl with diiodoethane at low temperature afforded **7**, which was obtained in 76% yield after workup. The ambient temperature reaction of **7** with TMSA (trimethylsilylacetylene) in Et_3N solution under Sonogashira conditions, using $[PdCl_2(PPh_3)_2]$ and CuI catalysts, resulted in exclusive reaction with the iodine substituent of **7** to give **8**, which was isolated in 77% yield.[15a,b] Although **8** was reactive toward a variety of arylethynes at elevated temperatures in the presence of the above catalysts, we found that the products of cross-coupling were formed in reduced yields, rarely clean, and often problematic to purify. We therefore converted **8** to the iodo analogue **9** via a second low-temperature lithium−halogen exchange reaction followed by treatment with diiodoethane. The enhanced reactivity of **9** compared to **8** toward Sonogashira cross-couplings was anticipated to result in enhanced yields and cleaner reaction products, an expectation that was confirmed during subsequent experimentation. Tetraethynylphenyl **10** was then selectively desilylated with K_2CO_3 in MeOH to give **11**,[16] which served as the core building-block for the construction of the required oligocruciforms **1**−**4**.

The cross-coupling reaction of ≥2 equiv of **9** with **11** in 6:1 toluene/Et_3N solution, using $[PdCl_2(dppf)]\cdot CH_2Cl_2$[17] and CuI catalysts, afforded 64% of oligo[3]cruciform **1** after workup. The employment of $[PdCl_2(PPh_3)_2]$ catalyst and pure Et_3N as solvent resulted in the formation of significantly reduced yields of **1**. In order to obtain optimal yields of **1**, it was also necessary to ensure complete exclusion of oxygen from the reaction. For example, one run was conducted under an atmosphere of 80:20 parts argon/air. In this case, oligo[4]cruciform **2** was isolated in 10% yield as a yellow powder with significantly reduced solubility compared to **1**, which was also obtained in 52% yield from the same reaction. An explanation consistent with the oxygen-assisted formation of **2** may be that a significant difference exists between the relative rates of palladium-catalyzed cross-coupling of each equivalent of **9** with the in situ generated organocuprate of **11**. The initial step in the reaction involves a fast cross-coupling between the organocuprate of **11** and the first equivalent of **9** to yield a triarylmonoethyne intermediate. However, in the presence of oxygen an alternative reaction pathway is available to this latter intermediate which involves the copper-catalyzed oxidative self-coupling of the remaining alkyne to afford **2**. The slower second cross-coupling reaction with **9** may therefore occur at a rate which is comparable to the oxidative self-coupling. Thus, in the presence of air, oxidative dimerization of the intermediate monoalkyne effectively competes with the second cross-coupling step, resulting in a mixture of **1** and **2**. Alternatively, comparable homo- and cross-coupling rates may lead to **2** via the initial coupling of two molecules of **11** followed by end-capping by **9**.[18a,b]

The formation of **2** is particularly surprising as it involves a multistep, one-pot generation of a 35 Å conjugated and insulated nanowire from simple monomeric starting materials. This observation further suggests that the reaction may become a

(13) For oligomeric enediynes and annulenes stabilized and solubilized with appended TIPS-ethynyl groups, see: (a) Boldi, A. M.; Anthony, J.; Gramlich, V.; Knobler, C. B.; Boudon, C.; Gisselbrecht, J.-P.; Gross, M.; Diederich, F. *Helv. Chim. Acta* **1995**, *78*, 779–796. (b) Anthony, J.; Boudon, C.; Diederich, F.; Gisselbrecht, J.-P.; Gramlich, V.; Gross, M.; Hobi, M.; Seiler, P. *Angew. Chem., Int. Ed. Engl.* **1994**, *33*, 763–766. (c) Anthony, J.; Knobler, C. B.; Diederich, F. *Angew. Chem., Int. Ed. Engl.* **1993**, *32*, 406–409. (d) Boldi, A. M.; Anthony, J.; Knobler, C. B.; Diederich, F. *Angew. Chem., Int. Ed. Engl.* **1992**, *31*, 1240–1242. For some dendritically branched phenyleneethynylenes with terminal TIPS-ethynyl groups, see: (e) Nierengarten, J.-F.; Zhang, S.; Gégout, A.; Urbani, M. *J. Org. Chem.* **2005**, *70*, 7550–7557.

(14) Tovar, J. D.; Swager, T. M. *J. Organomet. Chem.* **2002**, *653*, 215–222.

(15) (a) Takahashi, S.; Kuroyama, Y.; Sonogashira, K.; Hagihara, N. *Synthesis* **1980**, 627–630. (b) Sonogashira, K.; Tohda, Y.; Hagihara, N. *Tetrahedron Lett.* **1975**, 4467–4470.

(16) Marsden, J. A.; Miller, J. J.; Shirtcliff, L. D.; Haley, M. M. *J. Am. Chem. Soc.* **2005**, *127*, 2464–2476.

(17) Dierkes, P.; van Leeuwen, P. W. N. M. *J. Chem. Soc., Dalton Trans.* **1999**, 1519–1529.

(18) For the copper catalyzed oxidative self-coupling of ethynes, see, for example: (a) Batsanov, A. S.; Collings, J. C.; Fairlamb, I. J. S.; Holland, J. P.; Howard, J. A. K.; Lin, Z.; Marder, T. B.; Parsons, A. C.; Ward, R. M.; Zhu, J. *J. Org. Chem.* **2005**, *70*, 703–706. (b) Anderson, H. L. *Inorg. Chem.* **1994**, *33*, 972–981.

synthetically useful method for the direct generation of large conjugated nanowires if performed in air.

Oligo[3]cruciform **1** may serve as a central core for the further elaboration to longer [3 + 2*m*]cruciform oligomers (where *m* = integer). Thus, the selective deprotection of the trimethylsilyl groups of **1** using K_2CO_3 in 4:1 THF/MeOH afforded diethyne **3** in 94% yield after workup. It may be noted that the triisopropylalkynyl substituents on **3** and **11** result in an enhanced stabilization of the unsubstituted alkyne groups toward heat and light. Aromatic polyethynylbenzenes, in which the ethynes are unsubstituted, normally thermally polymerize or slowly degrade at ambient temperature and show a marked sensitivity to light. Compounds **3** and **11**, on the other hand, can be stored for several years in the dark at ambient temperature without any visible sign of decomposition and undergo only slight color darkening on exposure to indirect light for several months. As in the formation of **1** from **11** and **9**, the cross coupling of **3** with ≥2 equiv of **9** in toluene/Et_3N solution, using $[PdCl_2(dppf)]\cdot CH_2Cl_2$ and CuI catalysts, afforded 17% of oligo[5]cruciform **4** after workup. The low yield of **4** was principally attributed to its reduced solubility, which hampered purification. This latter observation is contrary to what was expected, i.e., that the longer oligomers would remain soluble. However, a decrease in solubility of longer TIPS-ethynyl functionalized enediyne oligomers in hexane has been observed by Diederich et al.[13]

The oligocruciforms **1**−**4** were characterized on the basis of mass spectroscopic, infrared, ^{1}H and ^{13}C NMR spectroscopic measurements, and spectral comparisons with their respective precursors. Due to the similarity in the chemical and magnetic environments of many of the protons and carbons in **1**−**4**, the NMR spectra always displayed some overlapping bands which hampered assignment. However, for each compound, particular groups of protons and carbons were numerically correctly represented, which supported characterization. Uniquely in the case of **1**, the ^{1}H NMR (Figure 1) displayed the expected number of peaks corresponding to the three TIPS and three aromatic protons, although situated in close proximity, as well as all nine peaks in its ^{13}C NMR due to the aromatic carbons. The assignment of the ^{1}H NMR of **1** was based on the expectation that the chemical shifts of the outer facing H3 and 5-TIPS protons of the terminal phenyl rings would be significantly different from those of the inner aromatic and TIPS protons. Accordingly, the magnetically and chemically most distinct singlets at 7.620 and 1.151 ppm were assigned to the outer phenyl H3 and 5-TIPS, respectively.

The assignment of the remaining closely situated peaks to the inner phenyl and TIPS protons was supported by NOESY and ROESY measurements. The ^{1}H NMR of the structurally similar **3** also displayed the three peaks expected for the aromatic protons as well as the 10 peaks in its ^{13}C NMR originating from the ethynyl carbons. The ^{1}H NMR spectrum of **2** exhibited four strong singlets due to the four chemically and magnetically inequivalent TIPS groups, and its ^{13}C spectrum displayed the expected 14 peaks corresponding to the ethynyl carbons and four peaks assignable to the four TIPS secondary carbons. As anticipated, oligo[5]cruciform **4** possessed the most complex NMR with the greatest number of overlapping peaks; however, five peaks corresponding to all five aromatic protons were clearly visible in its ^{1}H NMR. The characteristic signals assignable to the terminal TMS and ethynyl-H substituents were also correctly represented in the NMR spectra of **1**−**4**. ^{1}H NMR

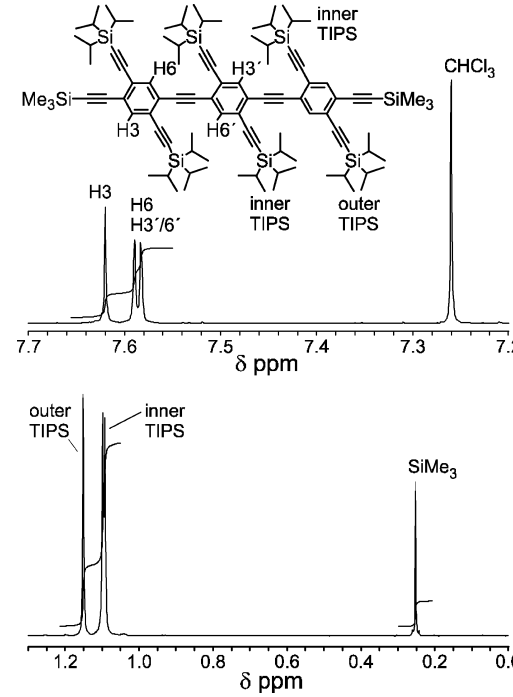

FIGURE 1. ^{1}H NMR of **1** showing expanded aromatic region (upper spectrum) and aliphatic region (lower spectrum). (As the aromatic region has been vertically enlarged relative to the aliphatic region, the integrations of the upper and lower spectral sections are not proportionate.)

dilution studies performed on the longest oligomer **4** and cycle **5** between, respectively, 4×10^{-7} and 5×10^{-6} mol/L in $CDCl_3$ and 1×10^{-6} and 1×10^{-5} mol/L in CD_2Cl_2 afforded only negligible changes in the chemical shifts, demonstrating that aggregation was either absent or unchanging over the concentration range studied, i.e., the range usual for NMR measurements.

The infrared spectra of **1**−**4** each exhibited a weak band within the range 2157−2161 cm^{-1} assignable to the ethynyl C≡C stretching vibration. In the case of **3**, the weak band at 3307 cm^{-1} was clearly assignable to the CH stretching mode of the terminal ethynyl ≡C−H groups.[19]

The clearest evidence for the oligocruciform identity of **1**−**4** was afforded by mass spectroscopic studies. Initial attempts at recording the ESI and MALDI-TOF mass spectra of **1**−**4** in the presence of various matrices and organic acids such as TFA failed to yield any peak clusters corresponding to those expected for the [M + H^+] molecular ions, presumably due to acid-mediated degradation of the oligocruciforms.

It is well known, however, that phenyleneethynylenes form complexes with Ag^+ and Cu^+ ions,[20a−c] which should be detectible by ESI and MALDI-TOF mass spectroscopy. However, the spectra of **1**−**4** mixed with $AgCF_3SO_3$ exhibited only very low intensity bands corresponding to the presence of [M + Ag^+] ions. The majority of peaks were assignable to the loss of TIPS substituents, and in the MALDI-TOF mass spectra, direct replacement of the TMS by Ag to afford the ethynylargentate. Clearly, the Ag^+ was causing significant desilylation

(19) Silverstein, R. M.; Webster, F. X. *Spectrometric Identification of Organic Compounds*, 6th ed.; J. Wiley & Sons, Inc.: New York, 1997.

(20) For the study and isolation of silver complexes with ethynes, see, for example: (a) Hellbach, B.; Rominger, F.; Gleiter, R. *J. Organomet. Chem.* **2006**, *691*, 1814–1816. (b) Létinois-Halbes, U.; Pale, P.; Berger, S. *J. Org. Chem.* **2005**, *70*, 9185–9190. (c) Schulte, P.; Behrens, U. *J. Organomet. Chem.* **1998**, *563*, 235–249.

under the mass spectral conditions.[21] However, the employment of $CuCF_3SO_3$ yielded significantly cleaner ESI and/or MALDI-TOF mass spectra with relatively intense [M + Cu^+] cluster peaks. Interestingly, the ESI technique only afforded [M + Cu^+] ions for the smaller oligomers **1** and **3**, while MALDI-TOF yielded [M + Cu^+] ions for all linear oligomers studied.

As mentioned earlier, we were interested in comparing the physical properties of the oligocruciforms with other similarly functionalized and sterically encumbered phenyleneethynylene nanostructures possessing alternative electronic conjugation pathways. Toward this goal, we prepared the ethynyl-TIPS-functionalized dehydrotribenzo[12]annulene **5** as shown in Scheme 2. Thus, key intermediate **13** was prepared from **12** via a five-step sequence as reported.[22] When treated with 1 equiv of *n*-BuLi in Et_2O at low temperature, **13** underwent a clean lithium−halogen exchange to the lithiophenyl, which was subsequently quenched with diiodoethane to afford **14** in 95% yield. The trimethylsilyl group of **14** could then be selectively removed using K_2CO_3 in 0.6:1 THF/MeOH to afford **15** in 98% yield after workup. Finally, addition of **15** to an excess of *t*-BuOCu in pyridine under argon yielded an organocuprate, which upon heating, underwent the Stephens−Castro cyclization to **5** which was isolated in 20% yield after purification.[23a−c] Upon treatment with ≥3 equiv of [(*n*-Bu)$_4$N]F in THF, the TIPS groups of **5** could be removed to provide the symmetrically functionalized triethynyldehydrotribenzo[12]annulene **16**, which after purification was obtained as a poorly soluble yellow solid in 94% yield. The latter macrocycle is a particularly interesting compound in that it may be anticipated to partake in Sonogashira-type cross-couplings with many readily available functionalized iodoaromatics, thereby serving as a key synthon for the creation of a wide variety of symmetrically trifunctionalized dehydrotribenzo[12]annulenes.[24a,b]

The dehydrotribenzo[12]annulenes **5** and **16** were characterized on the basis of mass spectroscopic, infrared, ^{1}H and ^{13}C NMR spectroscopic measurements. In contrast to the oligo[*n*]-cruciforms, the ESI technique afforded superior mass spectra for the macrocycles than did MALDI-TOF, with the [M + Cu^+] ions clearly visible in both cases. The ^{1}H NMR spectra, on the other hand, were particularly second order, comprising only two sets of multiplets in the aromatic region. The ^{13}C NMR spectra of **5** and **16**, however, displayed the correct number of peaks expected for such cyclic structures.

X-ray Crystal Structural Characterization of 1. In order to obtain detailed structural parameters of the oligo[*n*]cruciforms at a molecular level and determine the steric influence that the TIPS substituents exert on intermolecular interactions, we therefore determined the X-ray crystal structure of **1**, which served as a representative member of the series. Oligomer **1** crystallized with no included solvent in a monoclinic crystal system with the *C*2/*c* space group.

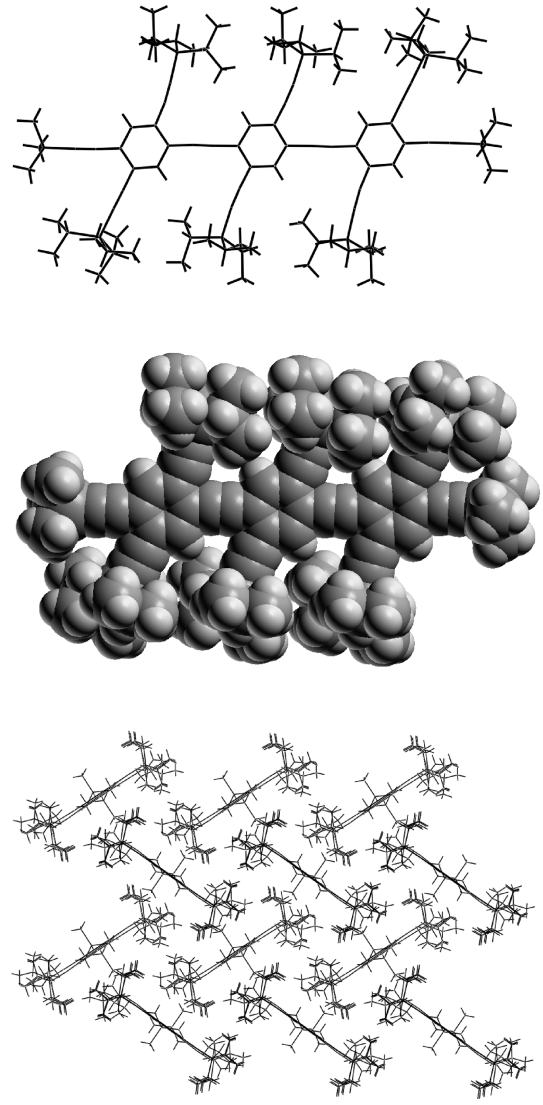

FIGURE 2. X-ray crystal structure of oligo[3]cruciform **1** (top: wireframe representation; center: spacefilling; bottom: packing motif as viewed down main axes of **1** molecules).

Despite the relatively large number of conformations available to **1** through twisting of the phenyl rings about its main axis, the molecule is essentially planar in the solid state with identical directional alignment of all phenyl rings with respect to each other (Figure 2, upper: wireframe; center: space-filling representations). The Si(TMS)−Si(TMS) distance is 25.5 Å, which places the molecule within the nanostructural domain. This preferred solid-state all-planar conformation has also been observed in the crystal structure of the related TIPS-functionalized linear tetraethynylethene trimer oligomers synthesized by Diederich and co-workers.[13b,d]

The three TIPS substituents within each row on either side of the molecule are in very close proximity and interdigitated with each another. In order to further accommodate this closeness of approach, the central TIPS-ethyne-phenyl-ethyne-TIPS moiety is partially bent into a slight S-shaped configuration, and each inner-terminal TIPS-ethyne substituent is slightly splayed out toward the TMS groups. Furthermore, the main axis of **1**, which passes through the three phenyl rings and TMS substituents, is not linear as expected but slightly curved into an S-shape, resulting from the combined effects of the sub-

(21) Yamamoto, Y. *Chem. Rev.* **2008**, *108*, 3199–3222.
(22) Tobe, Y.; Takaharu, H. *Jpn. Sci. Tech. Agency* **2005**−09−22, JP2005255778.
(23) For syntheses of unsubstituted dehydrotribenzo[12]annulene via the Stephens−Castro reaction, see: (a) Solooki, D.; Ferrara, J. D.; Malaba, D.; Bradshaw, J. D.; Tessier, C. A.; Youngs, W. J.; John, J. A.; Tour, J. M. *Inorg. Synth.* **1997**, *31*, 122–128. (b) Staab, H. A.; Graf, F. *Tetrahedron Lett.* **1966**, 751–757. (c) Campbell, I. D.; Eglinton, G.; Henderson, W.; Raphael, R. A. *Chem. Commun.* **1966**, 87–89.
(24) Dehydrobenzoannulenes functionalized with terminal ethynes are rare in the literature; see, for example: (a) Matzger, A. J.; Shim, M.; Vollhardt, K. P. C. *Chem. Commun* **1999**, 1871–1872. (b) Eickmeier, C.; Junga, H.; Matzger, A. J.; Scherhag, F.; Shim, M.; Vollhardt, K. P. C. *Angew. Chem., Int. Ed. Engl.* **1997**, *36*, 2103–2108.

stituent distortions described above and crystal packing factors (Figure 2, wireframe representation).

In the case of our series of oligo[*n*]cruciforms, it was of particular interest to determine whether the conjugated backbone of each molecule was effectively sterically isolated from its neighbors in the solid state due to the steric volume of the TIPS substituents.

The crystal lattice of **1** comprises two-dimensional layers, each 27 Å in thickness, within which the molecules of **1** are vertically packed together with the TMS groups forming the extreme upper and lower surfaces of every layer. The layers of **1** are also interdigitated with each other via the TMS substituents, with the shortest interlayer Si(TMS)−Si(TMS) distance of 6.376 Å. The steric volume of the trialkylsilyl substituents lining the upper and lower surface of each layer prevents any ethyne and phenyl contacts being formed between each layer. However, the interlayer domains are not tightly close-packed, as evidenced by some disorder within the terminal TIPS and TMS substituents which function as the interlocking groups lining the surface of each layer.

Within each layer, as defined by the plane through the *b*- and *c*-axes, the molecules of **1** are all tilted 66° in the same direction. The direction of tilting is also identical for all layers. When viewed down their main axes (i.e., 66° to the layer plane), the molecules of **1** are seen to be packed into a slipped herringbone motif (Figure 2, bottom: packing motif). The molecules of **1** therefore laterally slot together in an edge-to-face type arrangement, where the edge is defined by the row of three TIPS substituents on each side of **1** and the face is the axial cavity that lies between the two rows of TIPS groups in each molecule of **1**. In this way, each molecule is completely sterically isolated from its nearest neighbors by the TIPS substituents so that the conjugated ethynyl and phenyl parts of **1** are unable to form any intermolecular lateral contacts. Thus, within each layer, the shortest intermolecular phenyl−phenyl distance of 8.594 Å was found between C17 and H18 of the terminal phenyl rings. The shortest phenyl−phenyl interlayer distance was found to be 7.325 Å between the H21 hydrogens of the terminal phenyl rings. The X-ray crystal structure of **1** unambiguously demonstrates that the TIPS groups are of sufficient steric volume to prevent intermolecular $\pi-\pi$ contacts.

Electrochemical Properties. Both linear and cyclic conjugated oligomeric hydrocarbons functionalized with stabilizing and solubilizing ethynyl-TIPS groups have been the focus of electrochemical investigations due to their novel topologies and interesting electronic delocalization pathways.[13b,25a−c] We therefore considered that it would be of interest to perform some investigations into the electrochemical properties of selected members of our series of TIPS-ethynyl functionalized oligophenyleneethynylenes. Thus, the cyclic voltammetry of **1**, **5**, and **10** (Table 1 and Figure 3) was performed in CH_2Cl_2 in the presence of 0.1 mol/L of *n*-Bu_4NPF_6 and referenced against ferrocene as an internal standard. The cyclic voltammetry of cycle **5** at low scan rates exhibited two reversible reductions at −1.84 and −2.13 V vs Fc^+/Fc, with a cathodic/anodic peak separation ΔE_p of 60 and 100 mV, respectively.

The electrochemical properties of **5**, which is a Hückel-antiaromatic 12π electron system, are similar to those reported for the parent triangular hydrocarbon dehydrotribenzo[12]-annulene[25c] and a structurally related TIPS-protected dehydro-[18]annulene constructed from tetraethynylethene units,[25a] which also exhibited multiple reversible reductions, with E° for the first and second reductions of −1.12 and −1.52 V vs Fc^+/Fc, respectively. However, cycle **5** is more difficult to reduce than the TIPS-protected tetraethynylethene-based dehydro-[18]annulene, reflecting the longer cyclic conjugation pathway and greater number of π-electrons in the latter system, as well as the presence of an increased number of ethynyl-TIPS substituents, which are known to be stabilize the reduction process.[25b]

Interestingly, recent theoretical calculations on dehydrotribenzo-[12]annulene have also revealed that the electronic properties of this system are dominated by the individual aromaticity of the benzene rings rather than the antiaromatic contribution of the 12 π-electron circuit,[26] a factor which would also be expected to contribute to the difference in the electrochemical reduction propensities of **5** and the reported TIPS-protected dehydro[18]annulene.[25a]

The linear oligo[3]cruciform **1** also afforded two one-electron electron transfers at −1.86 and −2.04 V vs Fc^+/Fc; however, at low scan rates, only the first reduction was reversible, the second reduction becoming reversible at scan rates higher than 1 V s^{-1}. This latter behavior is characteristic of an electron transfer mechanism which triggers an irreversible chemical reaction. Increased scan rates ensure that the dianion is rapidly

TABLE 1. Electrochemical Data of 1 and 5 Observed by Cyclic Voltammetry (CV) in CH_2Cl_2 + 0.1 mol/L Bu_4NPF_6 (All Potentials Are Given versus Ferrocene, Used as Internal Standard)

oligomer/monomer	scan rate (V s^{-1})	E° ($V_{Fc+/Fc}$)	ΔE_p[a] (mV)
10	0.1	−2.25	100
1	0.1	−1.86	80
	>1.0	−2.04[b]	
5	0.2	−1.84	60
	0.2	−2.13	100

[a] ΔE_p is the potential difference between the cathodic and anodic peak potentials. [b] reversible electron transfer only at scan rates higher than 1 Vs^{-1}.

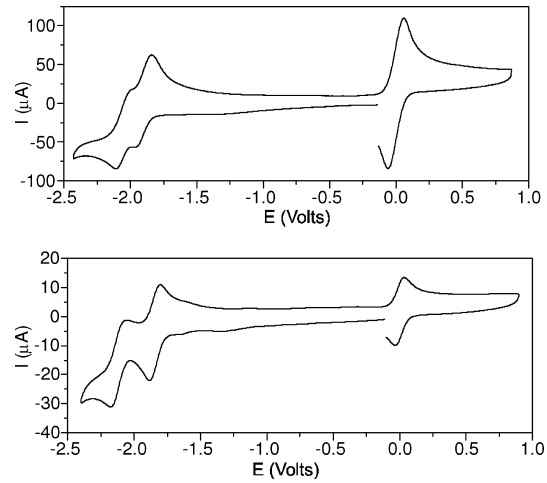

FIGURE 3. Cyclic voltammetry of **1** (1 V s^{-1} scan rate, upper) and **5** (0.2 V s^{-1} scan rate, lower voltammogram) in CH_2Cl_2 solution, with 0.1 mol/L of Bu_4NPF_6 in the presence of ferrocene.

(25) (a) Mitzel, F.; Boudon, C.; Gisselbrecht, J.-P.; Gross, M.; Diederich, F. *Chem. Commun.* **2002**, 2318–2319. (b) Boudon, C.; Gisselbrecht, J.-P.; Gross, M.; Anthony, J.; Boldi, A. M.; Faust, R.; Lange, T.; Philp, D.; Van Loon, J.-D.; Diederich, F. *J. Electroanal. Chem.* **1995**, *394*, 187–197. (c) Ferrara, J. D.; Tanaka, A. A.; Fierro, C.; Tessier-Youngs, C. A.; Youngs, W. J. *Organometallics* **1989**, *8*, 2089–2098.

(26) Tahara, K.; Yoshimura, T.; Sonoda, M.; Tobe, Y.; Williams, R. V. *J. Org. Chem.* **2007**, *72*, 1437–1442.

TABLE 2. UV−vis and Luminescence Emission Spectroscopic Data for 1−4 and 10 (Presented in Order of Increasing Oligomer Size) and Cycles 5 and 16

monomer/ oligomer	no. of aromatic rings (length, Å)	λ_{abs}[c] (nm)	$\lambda_{em\ solution}$ (nm)	$\lambda_{em\ solid}$ (nm)	$\lambda_{em\ solid}$[d] − $\lambda_{em\ solution}$[d] (nm)	optical bandgap E_g^{opt} (eV)[e]	quantum yield Φ
10	1 (12)[a]	274	346[d] 362	370[d]	24	3.5	0.18
3	3 (24)[b]	285	396[d] 416	434[d] 445	38	3.0	0.89
1	3 (26)[a]	286	399[d] 422	440[d] 453	41	2.9	0.93
2	4 (35)[a]	289	422[d] 447 462sh	467[d] 483	45	2.8	0.55
4	5 (39)[a]	287	417[d] 441	469[d] 486	52	2.8	0.76 (0.78)[g]
5	3	318	486 503[d] 514sh 537 542	516sh 539[d] 572	36	[f]	0.06
16	3	308	480 496[d] 505sh 527 533	504sh 539[d] 556sh 571sh	43	[f]	

[a] Si(TMS)−Si(TMS) distance. [b] H(alkyne)−H(alkyne) distance. [c] Absorption maximum of highest intensity. [d] Highest intensity emission peaks. [e] Determined from the lowest energy absorption edge of the thin film absorption spectrum. [f] Lowest energy absorption edge poorly defined. [g] Quantum yield in argon-degassed heptane. Unless otherwise stated, all UV−vis and luminescence solution measurements were performed in air-equilibrated heptane at 20−25 °C.

reoxidized before it can chemically react. The chemical reaction probably involves the protonation of the generated dianion by trace impurities of water. Indeed, dianions generated at such negative potentials are strong bases, and may react easily with residual water.

Somewhat surprisingly, the cyclic voltammetry of **2**, performed under conditions identical to those of **1** and **5**, showed no reduction processes either at relatively low scan rates or at scan rates >1 V s^{-1}. A possible contributory factor to this behavior may be related to the poor solubility of **2** in dichloromethane.

The first and second electrochemical reduction potentials of **1** and **5** are therefore strikingly similar despite their very different topologies, suggesting that their electrochemical properties are determined more by the presence and number of the benzene rings. It may be noted that both **1** and **5** possess the same number of benzene rings.

Diederich and co-workers[25b] have reported a TIPS-functionalized linear tetraethynylethene trimer oligomer, structurally related to **1**, for which the $E°$ for the first and second reduction potentials were −1.23 V (reversible) and −1.47 V (irreversible) vs Fc^+/Fc, respectively. Although the two systems exhibited the same number of reduction steps, the aromatic **1** was more difficult to reduce than Diederich's linear oligomeric tetraethynylethene analogue, following the same trend as in the macrocyclic systems discussed above. Interestingly, elongation of the axial conjugation by end-capping the tetraethynylethene trimer oligomer with phenyl rings, was found to increase its stability toward electrochemical reduction, affording three reductions at $E° = -1.17$, −1.42, and −2.00 V vs Fc^+/Fc, respectively.[13b,25b]

For comparison, the electrochemical properties of **10** were also measured (Table 1). It was found to afford only one well resolved reduction step at −2.25 V vs Fc^+/Fc, which was situated very close to the electrolyte discharge, and thereby preventing the observation of further reductions if present. Monomer **10** is therefore significantly more difficult to reduce than **1**. This behavior is consistent with the conjugation extension of **1**, which is expected to facilitate the first electron transfer.

From the above studies, it can therefore be seen that both **1** and **5** are able to undergo multiple electrochemical reductions, suggesting that these systems possess potential for the future development of electron reservoirs and capacitors within the field of molecular electronics. Further stabilization of the above TIPS-ethynyl functionalized phenyleneethynylene oligomers toward electrochemical reduction should also be possible upon selective functionalization with electron-withdrawing substituents and increasing the axial conjugation.

UV−vis Spectroscopic Properties. The spectroscopic properties of π-electron conjugated oligomers continue to be the focus of intensive studies in order to gain further insight into their electronic properties and to assess their potential as a reservoir of new materials with novel commercial applications. Within our series of phenyleneethynylene oligomers, it was important to determine the effect of the ethynyl-TIPS substituents and steric isolation upon the spectroscopic properties of these compounds. We therefore measured the UV−vis spectra of **1**−**5** and **16** in heptane solution over several concentrations from 6×10^{-5} to 9×10^{-7} mol/L and within the limits of experimental error showed no significant or progressive deviation from the Beer and Lambert law, demonstrating that aggregation was not occurring in dilute solution. The results of the UV−vis spectroscopic investigations are summarized in Table 2 and Figures 4 and 5.

As expected, upon increasing the conjugation length from cruciform **10** through oligo[3]cruciform **1** to oligo[5]cruciform **4**, the majority of the spectroscopic transitions move to lower energy as a result of the concomitant decrease in the HOMO−LUMO energy difference. The difference between the absorbance maxima of **1** and **4** is however considerably smaller than that between the maxima of **10** and **1**, indicating that the pentameric oligo[5]cruciform **4** is closely approaching the

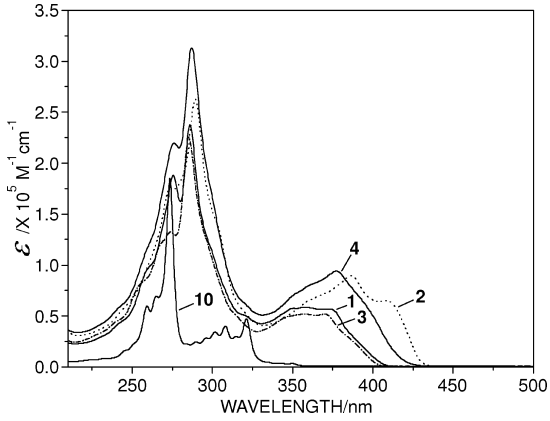

FIGURE 4. UV−vis spectra of oligo[*n*]cruciforms **1**−**4** and monomer **10** in heptane solution.

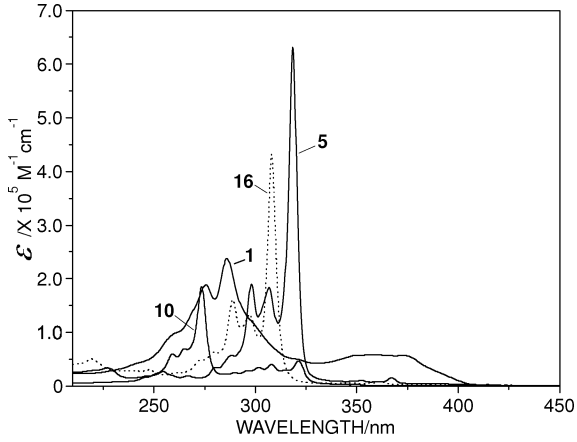

FIGURE 5. Comparison of UV−vis spectra of macrocycles **5** and **16**, oligo[3]cruciform **1**, and monomer **10** in heptane solution.

effective conjugation length for this system. This conclusion was also supported by the values of the optical energy gap (E_g^{opt}) of the linear oligomers (Table 2), in each case determined from the lowest energy absorption edge of the thin film absorption spectrum,[27a,b] which decreases in the order **10** ≫ **1** > **2** ≅ **4**.

Although **10** and **11** are structurally much simpler than either **1** or **4**, their UV−vis spectra were particularly complex and comprised three main domains. The first highest energy domain consisted of five to six transitions from 226 to 274 nm which increased successively in molar absorption coefficient, the lowest energy transition in this series being the most intense absorption in the spectrum. The second domain comprised seven peaks from 277 to 321 nm of intermediate molar absorption coefficients. The third and lowest energy domain comprised three to four absorptions from 322 to 350 nm with very low absorption coefficients characteristic of forbidden transitions.

The absorption peak separations in the UV−vis spectra of **10** and **11** varied between 5 and 15 nm, equating to the energies of vibrational transitions[28] and confirming that the complexity of the spectra originated from an enhanced degree of vibronic coupling.

In fact, all of the UV−vis spectra of **1**−**5** and **16** exhibited peaks or shoulders due to some vibronic coupling, although in

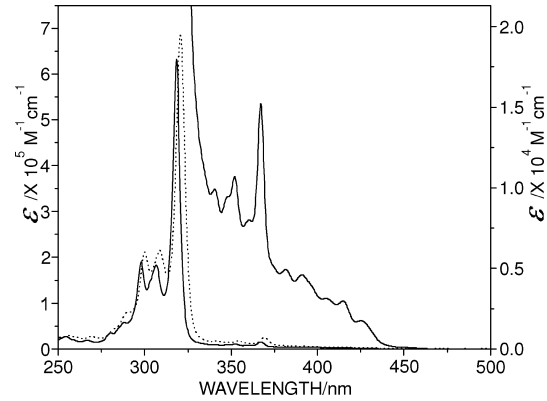

FIGURE 6. UV−vis spectra of **5** in heptane solution (solid curve, left) and 1:1 THF/DMSO (dotted curve, left) and magnification of the lower energy domain of **5** in heptane (solid curve, right).

1−**4** they were poorly resolved (Figures 4 and 5). For example, the second absorption domain in **10** which directly follows the most intense absorption peak merges into a single region of peaks or hill in the case of **1** and **4**. These findings are consistent with the degree of flexibility of the compounds investigated. Thus, the spectra exhibiting the greatest number of vibrational peaks are those of the rigid oligomers, i.e., **5**, **10**, **11**, and **16**, and those of the conformationally mobile **1**−**4** accordingly exhibit comparatively few clearly defined vibrational bands. Within the series of linear TMS-terminated compounds the molar absorption coefficients of the absorption maxima of greatest intensity also increase as expected in the order **10** < **1** < **4** from 1.86×10^5 (**10**) through 2.38×10^5 (**1**) to 3.13×10^5 M^{-1} cm^{-1} in the case of **4**.

The terminal TMS groups exert a small energy lowering effect upon the absorption maxima of the linear oligomers, as the absorption maxima within the region 280−420 nm move 1−4 nm to a shorter wavelength upon passing from **1** to the TMS-deprotected **3**. The electron-donating nature of the trialkylsilyl groups may therefore be raising the energy of the ground state HOMO, thereby reducing the HOMO−LUMO energy gap.

At wavelengths higher than 280 nm, the oligo[4]cruciform **2** exhibits the most red-shifted absorption spectrum within the series of linear oligomers, displaying a low energy absorption which tails well into the visible region at 445 nm. Elongation of the axial ethynyl bridges therefore results in a reduction of the π-electron HOMO−LUMO energy gaps of the tetraethynylphenyl-based oligo[*n*]cruciforms.

The UV−vis spectra of **1**−**5**, **10**, **11**, and **16** are slightly solvatochromic. For example, all compounds in THF solution exhibited small but significant 1 nm shifts in the majority of absorption maxima to lower energy. In the case of **5**, a further increase in the solvent polarity using 1:1 THF/DMSO resulted in 1−3 nm peak shifts to lower energy (Figure 6). Confirmation that the absorption shifts were not resulting from aggregation in these more polar solvents, was obtained by dilution studies which showed no significant or progressive deviation from the Beer and Lambert law. These findings suggest that the absorption maxima in the UV−vis spectra of the oligomers originate from $\pi-\pi^*$ transitions.[28]

As mentioned above, the macrocycles **5** and **16** afforded UV−vis spectra of greater similarity to that of **10** and **11** with respect to the sharpness and multiplicity of vibronic couplings. As in **10** and **11**, the UV−vis spectra of **5** and **16** each display a single sharp absorption of much higher intensity compared to

(27) (a) Steckler, T. T.; Abboud, K. A.; Craps, M.; Rinzler, A. G.; Reynolds, J. R. *Chem. Commun.* **2007**, 4904–4906. (b) Mühlbacher, D.; Neugebauer, H.; Cravino, A.; Sariciftci, N. S. *Synth. Met.* **2003**, *137*, 1361–1362.

(28) Turro, N. J. *Modern Molecular Photochemistry*; University Science Books: Herndon, VA, 1991.

the other peaks. These intense absorption peaks which occur at 318 nm in the UV−vis spectrum of **5** and at 308 nm in that of **16** exhibit very large molar absorption coefficients of 6.36×10^5 and 4.35×10^5 M^{-1} cm^{-1} respectively, compared to those of the most intense absorptions of the longest linear oligomers **2** and **4** at 289 nm (2.63×10^5 M^{-1} cm^{-1}) and 287 nm (3.13×10^5 M^{-1} cm^{-1}), respectively (Figure 4).

With respect to shape and the number of absorptions, the UV−vis spectra of **5** and **16** are virtually identical. However, the presence of the TIPS substituents significantly lower the energy of the absorption transitions, as is seen in the spectrum of **5** where all absorptions are red-shifted by 5−10 nm compared to those in the spectrum of **16**. The molar absorption coefficients of the three most intense absorptions in the UV−vis spectrum of **5** are also significantly enhanced (by 2.93×10^4−2.01×10^5 M^{-1} cm^{-1}) compared to those of **16**. Thus the sterically isolating TIPS substituents may result in an enhancement in the molar absorptivity of the dehydrotribenzo[12]annulene chromophore.

Interestingly, the most intensely absorbing peak in each of the UV−vis spectra of **5** and **16** exhibits considerable tailing on its lower energy edge which encompasses additional peaks of very low absorption coefficients. This unusual feature is most clearly observed in the case of **5**, where magnification of the UV−vis spectrum of a relatively concentrated solution in heptane (7.13×10^{-5} mol/L) revealed that the absorption tail comprised a suite of maxima presumably arising from vibronic coupling (Figure 6) and which finally disappeared into the baseline at 459 nm.[29]

Luminescence Spectroscopic Properties. A particularly characteristic physical property of oligophenyleneethynylenes is their enhanced luminescence when exposed to UV light. The color of the emission can be tuned by alterations in conjugation length and molecular topology, as well as by variation in the electronic properties and positions of appended substituents and functional groups. For this reason, oligophenyleneethynylenes have for example been utilized as emissive substrates in OLEDs.[4a,b]

In accord with the above considerations, we were therefore interested in the emissive properties of the sterically encumbered TIPS-functionalized oligophenyleneethynylenes **1**−**5** and the unhindered **16**, and observed that particular members of the series were indeed strongly luminescent when exposed to UV light both in solution and the solid state. The spectral emission data are summarized in Table 2, the luminescence spectra of **1**−**5** and **16** recorded in heptane solution shown in Figure 7, and spectra of the same compounds recorded as solvent-evaporated thin films are shown in Figure 8.

The solution luminescence spectra for all compounds were recorded over a range of concentrations from 5×10^{-4} to 9×10^{-7} mol/L and exhibited either negligible or zero changes in the shape and position of the emission maxima, showing that excited state aggregation was minimal in dilute solution. The emission spectra of each compound were also relatively unchanged upon excitation at high and low energy wavelengths

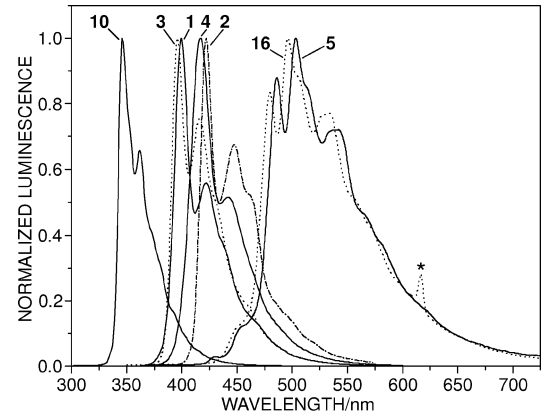

FIGURE 7. Normalized luminescence emission spectra of **1**−**5**, **10**, and **16** recorded in heptane solution. *2λ excitation scattering peak (see the Supporting Information for the respective excitation wavelengths and solution concentrations).

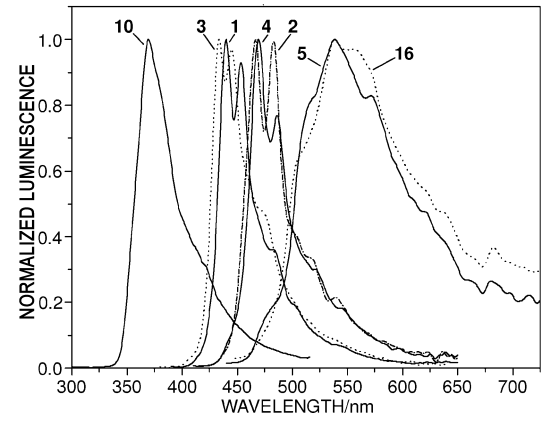

FIGURE 8. Normalized luminescence emission spectra of **1**−**5**, **10**, and **16** recorded as thin films.

corresponding to the absorption maxima of the respective UV−vis spectra (see the Supporting Information), revealing that reabsorption effects were not dominant in these systems.

The luminescence emission data (Table 2) reveal a general trend, i.e., that the highest intensity emission maxima of all compounds decrease in energy along the series **10** ≫ **3** > **1** > **4** > **2** ≫ **16** > **5** in solution and **10** ≫ **3** > **1** > **2** ≅ **4** ≫ **16** ≅ **5** in the solid state. Thus, within the series of linear oligomers both in solution and the solid state, the luminescence energy decreases and becomes more red-shifted with increase in conjugation length, and the macrocycles are emissive at much lower energies than the longest linear oligomers. This finding is in accord with the expected decrease in the gap between the excited state and ground state energy levels with increasing conjugation. As in the absorption spectra, the TMS groups of the linear oligomers and TIPS substituents of the macrocycles are exerting an electronic effect on the spectroscopic properties of these oligophenyleneethynylenes. Thus, removal of the terminal TMS groups results in a small increase in energy of the emission maxima upon passing from **1** to **3**. A similar effect is also observed in the solution luminescence spectra of the macrocycles where the emission energy of **16**, which lacks the TIPS substituents, is greater than that of **5**. This again reflects the electron donating nature of the trialkylsilyl groups which would be expected to raise the energy of the ground state HOMO and reduce the energy gap.

(29) The presence of this low energy tailing phenomenon resulted in a poorly defined absorption edge in the thin film UV−vis spectra of **5** and **16**, thereby introducing ambiguity in the measurement of E_g^{opt} for these compounds. The possibility exists that these comparatively weak absorptions may be the fingerprint of unidentified trace contaminants. However, cumulative evidence suggests otherwise. See for example the first report on the synthesis of dehydrotribenzo[12]-annulene, in which the UV−vis spectrum also clearly shows the presence of some weak absorptions on the lower energy edge of the principal maximum.[23c]

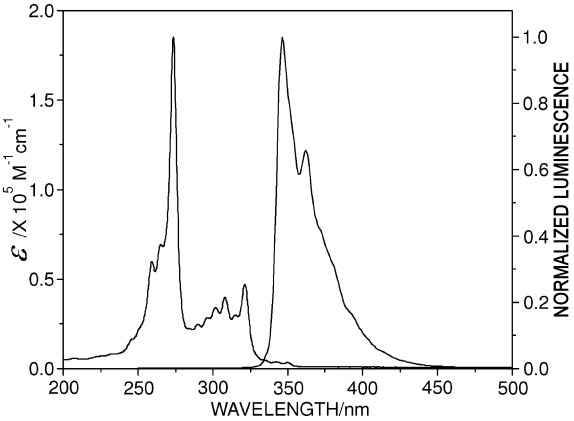

FIGURE 9. Comparison of the UV−vis spectrum (left) and normalized luminescence emission spectrum of **10** in heptane solution.

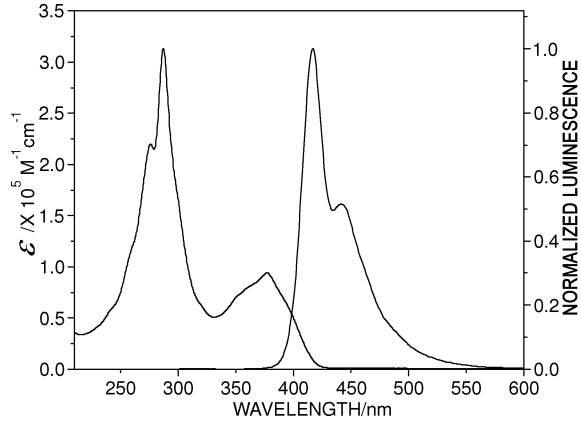

FIGURE 10. Comparison of the UV−vis spectrum (left) and normalized luminescence emission spectrum of oligo[5]cruciform **4** in heptane solution.

The solid state emissions for **1**−**5** and **16** are all of lower energy than the emissions in solution, with the energy difference between the $\lambda_{em\ solid}$ and $\lambda_{em\ soln}$ increasing in the following order, **10** < **1** < **4**, i.e., as the molecular size increases within the series of structurally most closely related linear oligomers. The values of the $\lambda_{em\ solid} - \lambda_{em\ soln}$ of the remaining oligomers **2**, **3**, **5**, and **16** is intermediate between that of **10** and **4**, averaging at 41 nm and therefore the same as that for **1**. Despite the steric isolation, an increased degree of exciton hopping is occurring in the solid state with increased radiationless energy loss prior to re-emission and a concomitant reduction in the energy of luminescence. This process would be expected to be augmented upon increasing the intermolecular contact surface area and molecular size. The larger $\lambda_{em\ solid} - \lambda_{em\ soln}$ value for **16** compared to **5** is also consistent with increased intermolecular contacts within the latter in the solid state due to the absence the TIPS substituents.

This latter conclusion is also supported by the finding that the thin film emission spectrum of **16** was of poorer resolution than that of **1**, suggesting that an increased amount of intermolecular interactions exists in the solid state of the former macrocycle.

As in the solution UV−vis spectra, the solution emission spectra of **1**−**5** and **16** all comprise multiple numbers of bands due to vibronic coupling, which is particularly well resolved in the case of cycles **5** and **16**, a finding that is consistent with their enhanced rigidity.[28]

The unsymmetric relationship between the shape of the solution absorbance and emission spectra in **1**−**5** and **16** introduces some ambiguity into the precise determination of the Stokes shifts of these compounds (see, for example, the spectra of **10** and **4** in Figures 9 and 10). A clarification of the absorption and emission bands that involve related transitions will require theoretical calculation of the spectra. However, comparison of the spectra does lead to a general conclusion, i.e., that the absorption and emission bands of the macrocycles **5** and **16** exhibit significantly greater separations than the linear oligomers, and have considerably broadened emissions. The relatively large apparent Stokes shifts of **5** and **16** suggest that dehydrotribenzo-[12]annulenes may have potential future applications as frequency downconversion materials.

Luminescence quantum yield estimations (Table 2) confirmed that the linear oligomers were strong fluorophores, and in particular the oligo[3]cruciforms **1** and **3**, which exhibited very high Φ values. Monomer **10** afforded an estimated quantum yield lower than those of the linear oligomers as expected, due to its comparatively small size and reduced degree of conjugation. However, the longest oligomers **2** and **4** exhibited lower quantum yields than the shorter oligo[3]cruciforms **1** and **3**. This effect has been previously noted for phenyleneethynylene oligomers.[30]

The butadiyne-bridged oligomer **2** was found to possess a lower quantum yield than **4**, suggesting that increasing the interphenyl ring separation and reducing the steric encumbrance of the oligomer may be detrimental to the strength of its luminescence. The possible existence of oxygen-quenching effects upon the luminescence of the oligomers was investigated in the case of the longest oligo[*n*]cruciform **4**. Thus, directly after measurement of the quantum yield of air-equilibrated solutions of **4**, the solutions were degassed with argon and the quantum yield redetermined. Although small compared to the inherent experimental errors, a slight increase in quantum yield from 0.76 to 0.78 was observed after argon degassing suggesting that some luminescence quenching by oxygen may occur in this system.

Somewhat surprisingly in view of its comparative rigidity and relatively large conjugation surface area, cycle **5** afforded the lowest luminescence quantum yield of all compounds studied, suggesting that dehydrotribenzo[12]annulenes may be inferior modules for the construction of strong fluorophores compared to the noncyclic analogues.

Thermochemical Properties. Polyacetylenic compounds are high energy materials with characteristic thermochemical properties that have been the subject of considerable interest over the past forty years. In particular, their thermally induced polymerizations, rearrangements and reactions have been widely exploited as an efficient and direct method of access to high

(30) Sudeep, P. K.; James, P. V.; Thomas, K. G.; Kamat, P. V. *J. Phys. Chem. A,* **2006**, *110*, 5642–5649.

(31) For topotactic polymerizations, see: (a) Tachibana, H.; Yamanaka, Y.; Sakai, H.; Abe, M.; Matsumoto, M. *Macromolecules* **1999**, *32*, 8306–8309, and references therein. Carbonization polymerizations: (b) Zhou, N.; Merschrod, E. F.; Zhao, Y. *J. Am. Chem. Soc.* **2005**, *127*, 14154–14155. (c) Kijima, M.; Tanimoto, H.; Shirakawa, H. *Synth. Met.* **2001**, *119*, 353–354. For explosive decompositions, see, for example: (d) de Meijere, A.; Kozhushkov, S.; Haumann, T.; Boese, R.; Puls, C.; Cooney, M. J.; Scott, L. T. *Chem.*−*Eur. J.* **1995**, *1*, 124–131.

(32) (a) Laskoski, M.; Steffen, W.; Morton, J. G. M.; Smith, M. D.; Bunz, U. H. F. *J. Am. Chem. Soc.* **2002**, *124*, 13814–13818. (b) Glezakou, V.-A.; Boatz, J. A.; Gordon, M. S. *J. Am. Chem. Soc.* **2002**, *124*, 6144–6152. (c) Dosa, P. I.; Erben, C.; Iyer, V. S.; Vollhardt, K. P. C.; Wasser, I. M. *J. Am. Chem. Soc.* **1999**, *121*, 10430–10431. (d) Boese, R.; Matzger, A. J.; Vollhardt, K. P. C. *J. Am. Chem. Soc.* **1997**, *119*, 2052–2053.

TABLE 3. DSC Data for 1, 3, 5, 11, and 16[a]

compd	T_{onset} (°C)	T_{max}[b] (°C)	$\Delta T_{1/2}$[c] (°C)	ΔH (kJ mol^{-1})
1	48	52	3	21[d]
	271	276	4	65
	278	307	26	−186
2	53	60	6	6[d]
3	247	258	13	−295
5	283	304	21	−316
11	169	174	3	29
	174	181	9	−171
16	157	176	27	−312

[a] Data obtained under an N_2 atmosphere (heating rate 2 °C/minute). [b] Maximum temperature of exo/endothermic peak. [c] Half-width of the exo/endothermic peak at T_{max}. [d] Reversible when heating terminated before passing through higher temperature transitions.

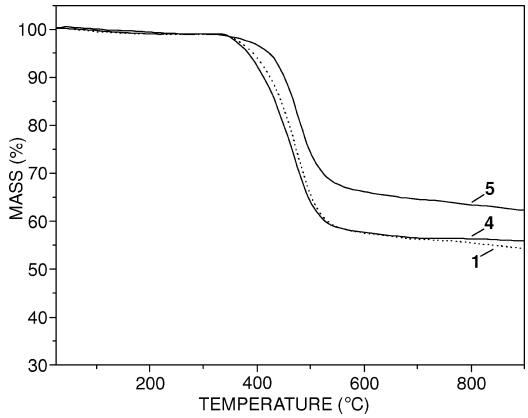

FIGURE 11. TGA curves for **1**, **4**, and **5** (10 °C/min heating rate).

carbon content polymers which would otherwise be difficult to prepare using conventional organic synthetic techniques. Depending upon heating rate and spatial orientations of the molecules within the crystal, a range of possible outcomes may be available to such materials upon heating, which include topotactic and amorphous carbonization polymerizations, or even explosive decomposition.[31a−d] A significant recent development concerning the latter behavior has been the discovery of carbon nanotubes in the residues remaining from the explosive decomposition of particular dehydroannulenes and metal-complexed phenyleneethynylenes.[32a−d] Phenyleneethynylenes become particularly unstable when the ethyne substituents are unfunctionalized. For example, in the case of cruciform-type molecules, 1,2,4,5-tetraethynylbenzene, the completely desilylated analogue of **10**, has been reported to explode upon heating.[33]

However, thermally unstable polyphenyleneethynylenes also often possess intrinsically interesting physicochemical properties in their own right, thus offering potential as new types of functional materials once their stability toward heat can be enhanced. In the light of these latter considerations, we performed differential scanning calorimetric (DSC) and thermogravimetric (TGA) measurements on selected oligo[*n*]cruciforms and dehydrotribenzo[12]annulenes in order to investigate their stability toward heat (Table 3 and Figures 11−13).

The DSC measurements showed that the larger TIPS-protected oligomers **1**, **3**, and **5** exhibited the greatest stability to heat, but with the macrocycles **5** and **16** involving exothermic energy changes of the greatest magnitude. After heating past the exotherm followed by cooling to ambient temperature, the

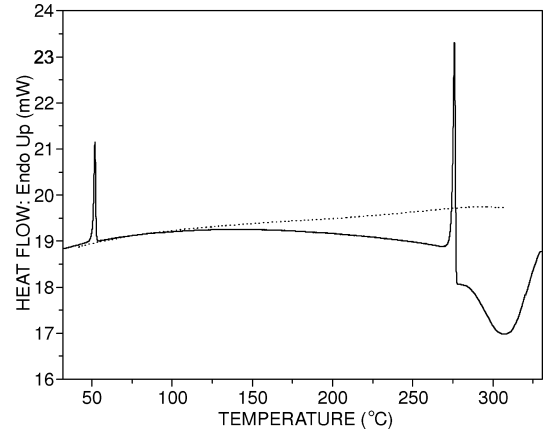

FIGURE 12. DSC heating trace of **1** (solid line), and reheating trace (dotted line) after passing through the 307 °C exotherm (2 °C/min heating rate).

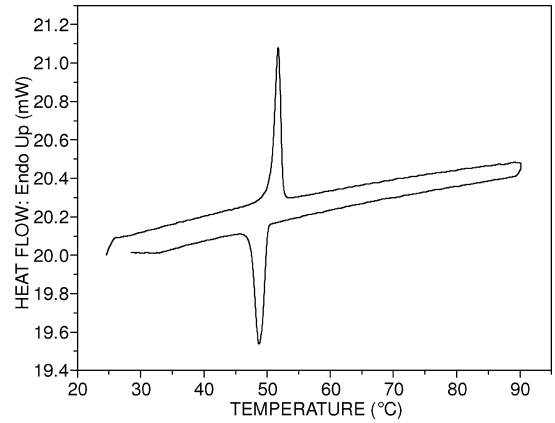

FIGURE 13. DSC heating curve of **1** showing reversible low temperature endothermic (T_{max} = 52 °C) and exothermic (T_{max} = 49 °C) transitions (2 °C/min heating rate).

original enthalpy changes were absent upon reheating in all compounds studied, demonstrating that the exothermic phase in each case involved an irreversible chemical reaction. The TGA measurements on oligomers **1**, **4**, and **5** (Figure 11) revealed that the onset of mass loss upon heating occurred at 340 °C, showing that at least in the cases of **1**, **4**, and **5**, the DSC exotherms and melting profiles were the signature of intramolecular chemical reactions or polymerizations rather than decompositions.

The DSC measurements of **3**, **5**, and **16** displayed a single exothermic peak. By contrast, the DSC of monomer **11** exhibited a sharp endothermic transition at 174 °C followed directly by a broader exothermic phase at 181 °C. This latter behavior is indicative of a melting transition which then develops into an irreversible chemical reaction. The DSC trace of **1** (Figure 12) is particularly interesting in that it displays two sharp endothermic transitions at 52 and 276 °C, respectively. The latter endotherm is directly followed by a broad exotherm at 307 °C in parallel to the behavior of **11**, signaling the onset of an irreversible chemical reaction. The endotherm at 52 °C is, however, reversible, as heating just past the endothermic transition followed by slow recooling to ambient temperature results in the development of a "mirror image" exothermic transition of similar enthalpy change but at a slightly lower temperature (Figure 13). Similarly, the DSC trace of **2** exhibited a weak reversible endothermic transition at 60 °C (Table 3). In

(33) Berris, B. C.; Hovakeemian, G. H.; Lai, Y.-H.; Mestdagh, H.; Vollhardt, K. P. C. *J. Am. Chem. Soc.* **1985**, *107*, 5670–5687.

the case of **2**, there were no further clearly definable transitions in the DSC trace up to 350 °C, in accordance with its visual melting behavior, which showed no changes other than gradual color-darkening over a wide temperature range (281−350 °C). The crystals of **1** and **2** exhibited no visible changes upon heating and cooling over the reversible low temperature DSC transitions, suggesting that they may originate from unusual crystal-to-crystal phase changes involving structural reorganization within the crystal networks.

As stated above, the DSC and TGA measurements support the conclusion that the apparent melting of oligomers **1** and **3**−**5** and monomer **11** (see the Experimental Section) is actually assignable to the onset of irreversible chemical reactions rather than simple melting behavior. A more detailed examination of the products from these high temperature transformations would be an avenue of future interest to determine if this is a route to new types of conjugated oligomers and polymers generated in the solid state. It may be noted that the visual and DSC transition temperatures appear to be sensitive to the heating rate, and increase in temperature as the heating rate is increased. This dependence accounts in part for the fact that the visual transitions occur at lower temperatures than the DSC transitions, the former of which being conducted at slower heating rates.

The high temperature thermal behavior of **1**, **4**, and **5** as measured by TGA, showed that continued heating from 340 °C resulted in mass reduction, signifying the onset of decomposition reactions. In the cases studied, the greatest loss in mass occurred between 340 and 570 °C. After 570 °C, the principal decomposition reaction had finished, with negligible mass changes up to 900 °C. The initial decomposition of **5** from 340 to 430 °C was slower than that of **1** and **4** and involved a 33% mass loss from 340 to 570 °C, whereas the oligo[*n*]cruciforms exhibited a 42% loss in mass over the same temperature range.

Thus, the thermochemical measurements revealed that the oligomer stability increases with increased TIPS and TMS functionalization. The stabilizing effects of the TIPS substituents suggests that this is a viable approach to the stabilization of otherwise thermally sensitive phenyleneethynylenes with potential materials applications.

Conclusion

A series of TIPS-substituted sterically encumbered oligo[*n*]-cruciform phenyleneethynylenes **1**−**4** constructed from tetraethynylbenzene units have been synthesized[34] and their physical properties compared to those of similarly functionalized cyclic analogue **5** and its desilylation product **16**. All oligophenyleneethynylenes were characterized by NMR, ESI, and/or MALDI-TOF mass spectroscopic measurements. The characterization of the oligomers as $[M + Cu^+]$ ions was found to be the cleanest and most effective method of mass spectral analysis of these systems. This technique may therefore be of general utility for the mass spectral characterization of nonpolar phenyleneethynylenes in cases when other approaches are unsuccessful. The steric isolation of the oligo[*n*]cruciforms was unambiguously demonstrated by the crystal structure of **1** which showed a complete absence of intermolecular contacts between the ethyne and phenyl subunits in the solid state.

Oligophenyleneethynylenes **1**−**5** and **16** all functioned as luminescent chromophores, and in particular the oligo[3]cruciforms **1** and **3** which exhibited particularly high quantum yields. UV−vis and luminescence spectroscopic dilution studies revealed that intermolecular associations between the conjugated parts of all oligomers were absent in dilute solution. However, thin film luminescence studies showed a significant red shifting in the emissions of all oligomers compared to those in solution, consistent with increased energy loss via intermolecular exciton hopping across the contacting TIPS substituents. The apparent Stokes shifts of the cycles **5** and **16** were surprisingly large compared to the longest oligo[*n*]cruciforms. Organic materials with large Stokes Shifts offer considerable potential as energy downconversion materials and luminescent concentrators in solar energy technology and as fluorescence labels for biomolecules.[35a,b] The unusually detailed vibronic coupling observed in the UV−vis and room temperature emission spectra of some of the oligophenyleneethynylenes and particularly in the UV−vis spectra of **10** and **11**, suggests that the spectroscopic properties of these compounds may be of theoretical interest.

Preliminary electrochemical studies showed that **1** and **5** were reversibly reducible, suggesting that they may possess future potential as electron reservoir materials upon further structural elaboration. The TIPS-protected oligomers also exhibited enhanced thermochemical and photochemical stability for polyethynylated-phenylenes, properties of particular importance for successful applications in molecular electronics.

Finally, with respect to the potential nanotechnological applications concerning controlled motions on surfaces,[11u] it may be of interest to note that oligo[*n*]cruciforms **1**−**4** are geared molecular systems. Rotation of a terminal phenyl ring about the linear axis of the oligo[*n*]cruciform will bring its ethynyl-TIPS substituents in contact with those of the adjacent ring, which are forced to rotate in the same direction. Propagation of this motion down the axis of the oligomer would result in unidirectional motion of all the ethynyl-TIPS substituents, thereby resulting in a geared molecular motion.

The spectrum of physicochemical properties exhibited by **1**−**5** and **16** suggests that further synthetic modifications via selective deprotection and Sonogashira-mediated functionalization will yield a rich diversity of structurally new polyconjugated oligo[*n*]cruciforms and dehydrotribenzo[12]annulene-based structures with potentially novel functions and molecular electronic/materials science applications. Work along these lines is currently underway.

Experimental Section

See the Supporting Information for general experimental methods, synthetic procedures and characterization data for **7**−**9**, **11**, **14**, and **15** and X-ray experimental data for **1**.

Electrochemistry. Electrochemical measurements were carried out in CH_2Cl_2 (with gentle degassing with argon) containing 0.1 mol/L of Bu_4NPF_6 in a classical three-electrode cell by cyclic voltammetry (CV). The working electrode was a glassy carbon disk (3 mm in diameter), the auxiliary electrode a Pt wire, and the pseudoreference electrode a Pt wire. The cell was connected to an Autolab PGSTAT20 potentiostat (Eco Chemie, Holland) driven by a GPSE software running on a personal computer. All potentials are given vs Fc^+/Fc used as internal reference and are uncorrected from ohmic drop. $E° = (E_{pa} + E_{pc})/2$ where E_{pa} and E_{pc} are the respective anodic and cathodic peak potentials.

(34) It may be noted that **1**−**4** do not constitute an exact homologous series due to the fact that **2** uniquely possesses a butadiene bridge. The "*n*" in oligo[*n*]cruciform is used in this work as a descriptor solely for the number of tetraethynylbenzene units within each oligomer, independent of the structural composition of the bridging units.

(35) (a) Peng, X.; Song, F.; Lu, E.; Wang, Y.; Zhou, W.; Fan, J.; Gao, Y. *J. Am. Chem. Soc.* **2005**, *127*, 4170–4171. (b) van Roosmalen, J. A. M. *Semiconductors* **2004**, *38*, 970–975.

Luminescence quantum yield estimations. The luminescence quantum yields[36] were calculated using the equation

$$\Phi_X = \Phi_{ST}(A_{ST}/A_X)(F_X/F_{ST})(\eta_X/\eta_{ST})^2$$

which can be rearranged to

$$\Phi_X = \Phi_{ST}(F_X/A_X)/(F_{ST}/A_{ST})(\eta_X/\eta_{ST})^2$$

where Φ is the luminescence quantum yield, A is the absorbance at the excitation wavelength, F is the area under the instrumentally corrected emission curve, η is the refractive index of the solvent, and subscripts ST and X refer to the standard and unknown, respectively. The function (F_X/A_X) is therefore the gradient of the plot of F_X verses A_X, which was determined from a series of dilute air-equilibrated heptane solutions with absorbances between 0.005 and 0.07 for each oligomer under investigation. Similarly, (F_{ST}/A_{ST}) was determined from the plot of F_{ST} verses A_{ST}, using anthracene in argon-degassed ethanol ($\Phi = 0.27$)[37] as the luminescence standard for compounds **1**−**4** and **10**. Quinine hemisulfate in 0.5 M aqueous H_2SO_4 ($\Phi = 0.546$ at 25 °C)[37] was used as the luminescence standard for the calculation of the quantum yield of **5**. We also used the quantum yield reported by Melhuish for deoxygenated ethanolic anthracene to calculate the quantum yield for air equilibrated ethanolic anthracene at ambient temperature, and found it to be in exact agreement with that determined by Venturi et al., i.e., $\Phi = 0.21$.[38] The experimental error associated with all determined quantum yield measurements (Table 2) was estimated to be within ± 10%.

Compound Syntheses. General Procedure for Sonogashira Heterocouplings. To the respective aryl iodide in the presence of a catalytic amount of $PdCl_2(PPh_3)_2$ or $[PdCl_2(dppf)]\cdot CH_2Cl_2$ under an atmosphere of argon was added by syringe Et_3N or toluene as solvent, followed by the appropriate alkyne reactant. After the mixture was stirred for 0.25 h, a solution of CuI in Et_3N, prepared in a separate argon-filled Schlenk, was syringed into the reaction, and stirring continued for 7−19 days at ambient temperature in the absence of light. A gray, brown, or yellow precipitate slowly formed in all cases, visually indicating the progress of the reaction. All solvent was then removed under reduced pressure on a water bath at 70 °C, and the residue isolated as described separately for each product.

Oligo[3]cruciform (1). Following the general procedure for Sonogashira couplings, a mixture of **11** (0.161 g, 3.31×10^{-4} mol), **9** (0.504 g, 7.63×10^{-4} mol), and $[PdCl_2(dppf)]\cdot CH_2Cl_2$ (0.030 g, 3.67×10^{-5} mol) in toluene (12 mL) and CuI (0.020 g, 1.05×10^{-4} mol) in Et_3N (2 mL) was stirred at ambient temperature for 14 d in the dark. All solvent was then removed under reduced pressure on a water bath and the residue extracted with boiling hexane (5 × 40 mL). The combined hexane extracts were chromatographed on a column of silica, eluting with hexane. The product thus obtained was suspended in absolute EtOH (250 mL) and the volume reduced to 90 mL with boiling and stirring. The suspension was then allowed to stand overnight, and the solid isolated by filtration under vacuum, washed with EtOH (3 × 2 mL), and air-dried to afford **1** (0.331 g, 64%) as an amorphous cream solid (mp = 252.0−255.0 °C). ^{1}H NMR ($CDCl_3$, 400.13 MHz, 25 °C): δ = 7.620 (s, 2H; outer phH3), 7.589 (s, 2H)/7.583 (s, 2H); {outer phH6/inner phH3′,6′}, 1.151 (s, 42H; outer 5-Si(CH(CH$_3$)$_2$)$_3$), 1.098 (s)/1.093 (s); {84H; outer 2-Si(CH(CH$_3$)$_2$)$_3$/inner 2′,5′-Si(CH(CH$_3$)$_2$)$_3$}, 0.252 ppm (s, 18H; Si(CH$_3$)$_3$). ^{13}C NMR ($CDCl_3$, 100.61 MHz, 25 °C): δ = 136.8, 136.3, 136.1, 125.4, 125.29, 125.26, 125.23, 125.14, 125.1, 104.0 (−C≡), 103.97 (−C≡), 103.9 (−C≡), 102.3 (−C≡), 100.6 (−C≡), 97.91 (−C≡), 97.88 (−C≡), 97.4 (−C≡), 92.6 (−C≡), 18.8 (CH(*C*H$_3$)$_2$), 18.7 (CH(*C*H$_3$)$_2$), 11.30 (*C*H(CH$_3$)$_2$), 11.26 (*C*H(CH$_3$)$_2$), −0.1 ppm (Si(CH$_3$)$_3$). UV/vis (heptane): λ_{max} (ε) = 242sh (42925), 260sh (97590), 276 (188988), 286 (238042), 320 (50598), 350 (57708), 358 (59268), 374 nm (56983 M^{-1} cm^{-1}). IR (thin film): 2942 (m), 2890 (w), 2864 (s), 2157 (w) (C≡C), 1490 (m), 1462 (m), 1250 (m), 1188 (m), 996 (m), 906 (m), 881 (vs), 840 (s), 768 (vs), 679 (s), 657 cm^{-1} (s). High res ESI MS *m*/*z*: 1551.9825 (5) [M$^+$], 1615.9138 (10) [M + Cu$^+$]. MALDI TOF MS *m*/*z*: 1615.82 (100) [M + Cu$^+$] calcd for $C_{98}H_{150}Si_8$ 1551.9910, $C_{98}H_{150}CuSi_8$ 1615.92.

Oligo[4]cruciform (2). Following the general procedure for Sonogashira couplings, a mixture of **11** (0.360 g, 7.39×10^{-4} mol), **9** (1.100 g, 1.66×10^{-3} mol), and $[PdCl_2(dppf)]\cdot CH_2Cl_2$ (0.068 g, 8.33×10^{-5} mol) in toluene (25 mL) and CuI (0.068 g, 3.57×10^{-4} mol) in Et_3N (8 mL) under an atmosphere of argon/air (approximately 80: 20) was stirred for 19 d in the dark. All solvent was then removed under reduced pressure on a water bath, the residue extracted with boiling hexane (3 × 50 mL), and the combined hexane extracts left to cool to ambient temperature. The mixture was gravity filtered in order to separate the suspended yellow solid which formed upon cooling and the filtrate reduced in volume to 20 mL under reduced pressure on a water bath. The filtrate was then purified by chromatography and EtOH treatment as described above to yield **1** (0.598 g, 52%). The yellow solid was boiled in hexane (60 mL) and the hot mixture gravity filtered. The filtrate was concentrated by continued boiling to 20 mL and allowed to cool to ambient temperature. The solid which formed was isolated by filtration under vacuum, washed with hexane (2 × 1 mL), and then recrystallized three times from hexane to afford **2** (0.076 g, 10%) as a bright yellow solid after air drying. (mp: microcrystals darken to an amber-brown color from 281.0−287.0 °C but remain transparent. Color-darkening continues up to the heating limit of 350 °C with no observable melting transitions). ^{1}H NMR ($CDCl_3$, 400.13 MHz, 25 °C): δ = 7.609 (s, 2H; phH), 7.583 (s, 4H; phH), 7.568 (s, 2H; phH), 1.166 (s, 42H; Si(CH(CH$_3$)$_2$)$_3$), 1.153 (s, 42H; Si(CH(CH$_3$)$_2$)$_3$), 1.112 (s)/1.110 (s); {84H; Si(CH(CH$_3$)$_2$)$_3$}, 0.251 ppm (s, 18H; Si(CH$_3$)$_3$). ^{13}C NMR ($CDCl_3$, 100.61 MHz, 25 °C): δ = 136.9, 136.7, 136.2, 135.8, 126.3, 125.7, 125.46, 125.44, 125.2, 124.8, 124.5, 103.96 (−C≡), 103.93 (−C≡), 103.8 (−C≡), 103.3 (−C≡), 102.3 (−C≡), 100.7 (−C≡), 98.7 (−C≡), 98.3 (−C≡), 97.9 (−C≡), 97.4 (−C≡), 93.4 (−C≡), 92.5 (−C≡), 81.3 (−C≡), 79.7 (−C≡), 18.8 (CH(*C*H$_3$)$_2$), 18.69 (CH(*C*H$_3$)$_2$), 18.66 (CH(*C*H$_3$)$_2$), 11.32 (*C*H(CH$_3$)$_2$), 11.30 (*C*H(CH$_3$)$_2$), 11.28 (*C*H(CH$_3$)$_2$), 11.2 (*C*H(CH$_3$)$_2$), −0.1 ppm (Si(CH$_3$)$_3$). UV/vis (heptane): λ_{max} (ε) = 274 (176727), 289 (263185), 300sh (149680), 359 (63832), 387 (89395), 408 nm (65036 M^{-1} cm^{-1}). IR (thin film): 2942 (m), 2890 (w), 2864 (m), 2158 (w) (C≡C), 1485 (m), 1462 (m), 1397 (m), 1250 (m), 1187 (m), 996 (m), 904 (m), 874 (vs), 853 (s), 842 (s), 769 (s), 735 (m), 677 (s), 660 cm^{-1} (vs). MALDI TOF MS *m*/*z*: 2101.19 (100) [M + Cu$^+$], calcd for $C_{130}H_{194}CuSi_{10}$ 2101.22.

Oligo[3]cruciform (3). To a solution of **1** (0.598 g, 3.85×10^{-4} mol) in THF (36 mL) and MeOH (9 mL) was added powdered K_2CO_3 (0.159 g, 1.15×10^{-3} mol) and the mixture stirred at ambient temperature in the dark for 7 d. All solvent was then removed under reduced pressure at ambient temperature to yield a white solid which was extracted with boiling hexane (4 × 30 mL). The combined hexane extracts were then added to a column of silica, which was first washed with some hexane and then eluted with 2% Et_2O/hexane. The product thus obtained was then recrystallized from boiling hexane (40 mL) to afford **3** (0.511 g, 94%) as a microcrystalline white powder after air drying. (mp: crystals transform into a partly melted amber-colored glass at 227.0 - 228.0 °C, with no further change other than color-darkening up to the heating limit of 350 °C). ^{1}H NMR ($CDCl_3$, 400.13 MHz, 25

(36) Fery-Forgues, S.; Lavabre, D. *J. Chem. Educ.* **1999**, *76*, 1260–1264.
(37) Melhuish, W. H. *J. Phys. Chem.* **1961**, *65*, 229–235.
(38) Venturi, M.; Marchioni, F.; Balzani, V.; Opris, D. M.; Henze, O.; Schlüter, A. D. *Eur. J. Org. Chem.* **2003**, 4227–4233. The quantum yield of anthracene in air-equilibrated ethanol ($\Phi = 0.21$) was determined by the group of Venturi, who found that their value agrees with the quantum yield ($\Phi = 0.27$) of anthracene in de-aerated ethanol reported by Melhuish, as well as the rate constant for the oxygen quenching published by the latter author. We thank Professor Margherita Venturi for this information.

°C): δ = 7.626 (s, 2H; phH), 7.617 (s, 2H; phH), 7.608 (s, 2H; phH), 3.343 (s, 2H; −C≡CH), 1.145 (s, 42H; Si(CH(CH$_3$)$_2$)$_3$), 1.106 ppm (s, 84H; Si(CH(CH$_3$)$_2$)$_3$). ^{13}C NMR (CDCl$_3$, 100.61 MHz, 25 °C): δ = 136.4, 136.1, 135.8, 125.9, 125.5, 125.3, 125.2, 124.7, 103.9 (−C≡), 103.88 (−C≡), 103.6 (−C≡), 98.2 (−C≡), 97.9 (−C≡), 97.87 (−C≡), 92.8 (−C≡), 92.6 (−C≡), 82.9 (−C≡), 81.3 (−C≡), 18.7 (CH(*C*H$_3$)$_2$), 11.28 (*C*H(CH$_3$)$_2$), 11.25 ppm (*C*H(CH$_3$)$_2$). UV/vis (heptane): λ_{max} (ε) = 256sh (82714), 269sh (123070), 274 (132814), 285 (226223), 347 (49597), 356 (51683), 370 nm (51604 M^{-1}cm^{-1}). IR (thin film): 3307 (w) (≡C−H), 2941 (m), 2889 (w), 2863 (m), 2159 (w) (C≡C), 1489 (m), 1461 (m), 1402 (m), 1187 (m), 997 (m), 902 (s), 880 (s), 868 (vs), 769 (s), 730 (s), 674 (vs), 662 (vs), 650 cm^{-1} (vs). High res ESI MS *m*/*z*: 1471.8226 (100) [M + Cu$^+$]. MALDI TOF MS *m*/*z*: 1471.83 (70) [M + Cu$^+$], calcd for $C_{92}H_{134}CuSi_6$ 1471.84.

Oligo[5]cruciform (4). Following the general procedure for Sonogashira couplings, a mixture of **3** (0.050 g, 3.55 × 10^{-5} mol), **9** (0.063 g, 9.53 × 10^{-5} mol), and [PdCl$_2$(dppf)]·CH$_2$Cl$_2$ (0.009 g, 1.10 × 10^{-5} mol) in toluene (9 mL) and CuI (0.012 g, 6.30 × 10^{-5} mol) in Et$_3$N (1.5 mL) was stirred at ambient temperature for 4 d in the dark and then at 60 °C for 5 d. All solvent was then removed under reduced pressure on a water bath, the residue extracted with boiling heptane (3 × 10 mL), and the combined heptane extracts chromatographed on a column of Silica eluting with heptane. When the product was sufficiently separated from the more slowly moving contaminants (as visualized with a fluorescent lamp operating at 312 nm), the latter were dug out from the column, and the crude **4** isolated by elution with 2% Et$_2$O/heptane. The product was then rechromatographed on Silica with 5%CH$_2$Cl$_2$/hexane and after isolation from the eluate, boiled in absolute EtOH (10 mL). The mixture was allowed to cool to ambient temperature and the suspended solid isolated by filtration under vacuum, washed with absolute EtOH (3 × 1 mL), and then treated in the same way with *n*-propanol to afford **4** (0.015 g, 17%) as a bright yellow solid after air drying. (mp: slow transformation into an amber-colored glass from 235.1 to 243.5 °C, which color-darkened up to the heating limit of 330 °C). ^{1}H NMR (CDCl$_3$, 400.13 MHz, 25 °C): δ = 7.640 (s, 2H; phH), 7.635 (s, 2H; phH), 7.631 (s, 2H; phH), 7.594 (s, 2H; phH), 7.586 (s, 2H; phH), 1.153 (s, 42H; Si(CH(CH$_3$)$_2$)$_3$), 1.105 (s, 126H; Si(CH(CH$_3$)$_2$)$_3$), 1.098 (s, 42H; Si(CH(CH$_3$)$_2$)$_3$), 0.253 ppm (s, 18H; Si(CH$_3$)$_3$). ^{13}C NMR (CDCl$_3$, 100.61 MHz, 25 °C): δ = 136.8, 136.3, 136.1, 125.4, 125.3, 125.28, 125.26, 125.23, 125.12, 125.05, 103.98 (−C≡), 103.96 (−C≡), 103.91 (−C≡), 102.3 (−C≡), 100.6 (−C≡), 97.9 (−C≡), 97.3 (−C≡), 92.76 (−C≡), 92.74 (−C≡), 92.65 (−C≡), 92.63 (−C≡), 18.8 (CH(*C*H$_3$)$_2$), 18.7 (CH(*C*H$_3$)$_2$), 11.28 (*C*H(CH$_3$)$_2$), 11.26 (*C*H(CH$_3$)$_2$), −0.1 ppm (Si(CH$_3$)$_3$). UV/vis (heptane): λ_{max} (ε) = 276 (219907), 287 (313112), 377 nm (94174 M^{-1}cm^{-1}). IR (thin film): 2942 (m), 2890 (w), 2864 (m), 2161 (w) (C≡C), 1493 (m), 1461 (m), 1401 (m), 1250 (m), 1187 (m), 997 (m), 903 (m), 881 (vs), 858 (s), 841 (s), 768 (vs), 677 (s), 659 cm^{-1} (vs). MALDI TOF MS *m*/*z*: 2537.52 (100) [M + Cu$^+$], calcd for $C_{158}H_{238}CuSi_{12}$ 2537.52.

4,4′,4″-Tris(triisopropylsilylethynyl)dehydrotribenzo[12]annulene (5). To a dried, argon -filled 25 mL 2-necked flask fitted with a reflux condenser vacuum/argon inlet adaptor and rubber septum, and containing CuCl (0.104 g, 1.05 × 10^{-3} mol) and *t*-BuOK 0.117 g, 1.04 × 10^{-3} mol), was added N$_2$-purged pyridine (6 mL) via syringe. The reaction was stirred at ambient temperature for 0.5 h, and then **15** (0.200 g, 4.90 × 10^{-4} mol) added by syringe. With continued stirring, the resulting orange-red suspension was heated at 35−40 °C for 4 h and then at 125 °C−140 °C for 10 h during which time the color changed to brown. After heating, the pyridine was removed by distillation under reduced pressure on a water bath at 35 °C and the black residue extracted with heptane (4 × 200 mL). Removal of the heptane by distillation on a water bath yielded a beige solid which was chromatographed on two successive columns of silica, eluting with heptane, to afford **5** (0.028 g, 20%) as a bright yellow solid after air-drying. In some runs, further purification was necessary, either by repeated chromatography as above, or by brief ultrasonication in *n*-propanol, isolation by filtration under vacuum, washing with *n*-propanol (3 × 2 mL), and air drying. (mp = 270.5−274.5 °C transforming to an amber glass which slowly darkened in color up to the heating limit of 310 °C). ^{1}H NMR (CD$_2$Cl$_2$, 400.13 MHz, 22 °C): δ = 7.451 (t, 3H; H3), 7.298 (d, 6H; H5, H6), 1.137 ppm (m, 63H; Si(CH(CH$_3$)$_2$)$_3$). ^{13}C NMR (CD$_2$Cl$_2$, 100.61 MHz, 22 °C): δ = 135.9, 132.63, 132.59, 127.1, 126.5, 124.7, 105.9 (−C≡), 94.7 (−C≡), 94.1 (−C≡), 93.4 (−C≡), 19.0 (CH(*C*H$_3$)$_2$), 11.8 ppm (*C*H(CH$_3$)$_2$). UV/vis (heptane): λ_{max} (ε) = 227 (33526), 254 (27002), 267 (18988), 280 (34750), 288 (57485), 298 (190345), 307 (182985), 318 (636242), 367 nm (15168 M^{-1}cm^{-1}). IR (thin film): 2941 (m), 2890 (w), 2864 (m), 2142 (w) (C≡C), 1490 (m), 1462 (m), 995 (m), 940 (m), 887 (s), 881 (s), 823 (s), 793 (s), 705 (vs), 676 (vs), 656 cm^{-1} (vs). High res ESI MS *m*/*z*: 903.4162 (100) [M + Cu$^+$], 1745.9004 (9) [2M + Cu$^+$], calcd for $C_{57}H_{72}CuSi_3$ 903.4232.

4,4′,4″-Triethynyldehydrotribenzo[12]annulene (16). To a solution of **5** (0.127 g, 1.51 × 10^{-4} mol) in THF (20 mL) was added *n*-Bu$_4$NF (1.0 M solution in THF; 0.60 mL, 6.00 × 10^{-4} mol) and the solution stirred at ambient temperature in the dark for 48 h. All solvent was then removed under reduced pressure at ambient temperature, MeOH (15 mL) added to the residue, and the suspension briefly ultrasonicated and filtered under vacuum. The isolated solid was washed with MeOH (4 × 5 mL), air-dried, dissolved in warm CH$_2$Cl$_2$ (100 mL), and chromatographed on a column of silica, eluting with CH$_2$Cl$_2$. The product obtained from the chromatography was finally suspended in CH$_2$Cl$_2$ (5 mL), briefly ultrasonicated, and filtered under vacuum and the isolated solid washed with CH$_2$Cl$_2$ (3 × 0.5 mL) and air-dried to yield **16** (0.053 g, 94%) as a fibrous yellow solid. (mp: color-darkening was observed from 160.0 to 169.0 °C, but no melting phase up to the heating limit of 200 °C). ^{1}H NMR (CD$_2$Cl$_2$, 500.13 MHz, 25 °C): δ = 7.476 (m, 3H; H3), 7.328 (m, 6H; H5, H6), 3.268 ppm (s, 3H; −C≡CH). ^{13}C NMR (CD$_2$Cl$_2$, 100.61 MHz, 24 °C): δ = 136.0, 132.9, 132.7, 127.13, 127.08, 123.5, 94.1 (−C≡), 93.3 (−C≡), 82.5 (−C≡), 80.3 ppm (−C≡). UV/vis (heptane): λ_{max} (ε) = 219 (50738), 248 (30009), 273 (48527), 280 (63223), 289 (161041), 297 (134079), 308 (435119), 347 (6108), 362 nm (8398 M^{-1}cm^{-1}). IR (thin film): 3290 (m) (≡C−H), 3258 (s) (≡C−H), 1488 (s), 902 (s), 890 (s), 836 (m), 826 (vs), 664 (vs), 635 (s), 610 (vs), 604 cm^{-1} (vs). High res ESI MS *m*/*z*: 372.0897 (100) [M$^+$], 435.0196 (30) [M + Cu$^+$], calcd for $C_{30}H_{12}Cu$ 435.0230.

Acknowledgment. The Centre National de la Recherche Scientifique and the Institut Charles Sadron are acknowledged for financial support (P.N.W.B.) and the Ministère de l'Enseignement Supérieur et de la Recherche is acknowledged for a PhD fellowship (A.A.). Raymonde Baltenweck-Guyot and Romain Carriere of the Service de Spectrometrie de Masse are thanked for the MALDI and ESI mass spectrometric measurements. Y. Guilbert of the ICS is thanked for the TGA measurements, Professor Mir Wais Hosseini is thanked for the use of the DSC, and Dr. Sylvie Ferlay is thanked for the DSC measurements. Dr. Marie-Thérèse Youinou is thanked for constructive comments.

Supporting Information Available: General experimental methods, synthetic procedures, and characterization data for **7**−**9**, **11**, **14**, and **15**, UV−vis spectral data for **10**, ^{1}H and ^{13}C spectra of **1**−**5**, **7**−**9**, **11**, **14**−**16**, X-ray experimental data for **1** and full page thermal ellipsoid plot of **1**. This material is available free of charge via the Internet at http://pubs.acs.org.

JO802797E